ZONE CONTROLLER AND

DETECTOR LOCATIONS AT BRUCE B

By

Ioannis A. Anastasiou

PART B: INDUSTRIAL PROJECT

A project report submitted in partial fulfillment of

the requirements for the degree of

Master of Engineering

The work reported upon herein was undertaken at

Atomic Energy of Canada Limited, Sheridan Park, Ontario

Department of Engineering Physics

McMaster University

Hamilton, Ontario

MASTER OF ENGINEERING
(Engineering Physics)

McMASTER UNIVERSITY
Hamilton, Ontario

TITLE (PART B): Zone Controller and Detector Locations at Bruce B

AUTHOR: Ioannis A. Anastasiou

SUPERVISOR: Dr. O. A. Trojan

NUMBER OF PAGES: ix, 53.

ABSTRACT

The objective of this study was to investigate the effectiveness of various arrangements of zone controller and detector locations in suppressing xenon induced spatial power oscillations. Using the SORGHUM code, which is a two-group neutron diffusion code, it was necessary to modify the cross sections set as taken from the more detailed CHEBY code. Then, the optimum axial location of the zone controllers was investigated with a three-dimensional study, while later a two-dimensional search in detail revealed the optimal radial locations of the zone controllers and the detectors associated with them.

ACKNOWLEDGEMENTS

I wish to express my appreciation and gratitude for the assistance and stimulation provided throughout this study by Dr. O. A. Trojan and Dr. P. Akhtar of the Reactor Division of Atomic Energy of Canada Limited.

My deep appreciation is also forwarded to Dr. V. K. Mohindra and Mr. M. Mamourian, also of AECL, for the constructive discussions I had with them.

CONTENTS

		PAGE
1.	INTRODUCTION	1
2.	DERIVATION OF THE CROSS SECTION	1
3.	THREE-DIMENSIONAL SEARCH	4
4.	TWO-DIMENSIONAL SEARCH	7
	REFERENCES	11

LIST OF TABLES

TABLE	
1	Incremental absorption cross sections used in the simulations with the CHEBY code.
2	"Supercell" properties from discrete adjuster properties.
3	Material properties for Bruce B.
4	Comparison between steady state thermal flux distributions obtained in SORGHUM and CHEBY.
5	Ratio of thermal flux at the various cells with the zone controllers at z = 8. The first controller is empty.
6	Ratio of thermal flux at the various cells with the zone controllers at z = 9. The first controller is empty.
7	Transients of the thermal flux at the detector locations of control region #1, due to a refuelling perturbation.
8	Transients of the thermal flux at the detector locations of control region #2, due to a refuelling perturbation.
9	Transients of the thermal flux at the detector locations of control region #3, due to a refuelling perturbation.
10	Transients of the thermal flux at the detector locations of control region #4, due to a refuelling perturbation.
11	Transients of the 1-4 tilt (%) for various zone controller-detector configurations.
12	Transients of the 1-4 tilt (%) due to a refuelling perturbation, with spatial control, and for three different radial controller locations.
13	Transients of the 1-4 tilt (%) due to a xenon perturbation, with spatial control, and for three different radial controller locations.

TABLE

14	Transient of the maximum thermal flux due to a xenon perturbation, trying to keep the zonal power constant.
15	Transient of the 1-4 tilt (%) due to a xenon perturbation, with zone filling in steps.
16	Steady state power ratios at various cells around controller #1, after emptying the controller.
17	Steady state power ratios at various cells around controller #1, after xenon perturbation.
18	The values of TABLE 17 after being normalized to the power ratio used for TABLE 16.
19	The differences between the values listed on TABLES 16 and 18.
20	The time response, 1-4 tilt (%), of various pairs of detectors examined, due to a xenon perturbation.
21	The flux ratio after emptying the controller #1 and the maximum 1-4 tilt (%) for each detector locations examined.

LIST OF FIGURES

FIGURE	
1	Quadrant core model with no adjusters (front view).
2	Quadrant core model with adjusters (fron view).
3	Octant core model (top view).
4	Relationships between "supercell" and discrete adjuster properties.
5	The fundamental mode at steady state.
6	The first axial mode at steady state.
7	The first azimuthal mode (top to bottom) at steady state.
8	The first azimuthal mode (side-to-side) at steady state.
9	Quadrant core model (front view) with detectors 1A and 4A.
10	Quadrant core model (front view) with detectors 1B, 1C, 4B and 4C.
11	Quadrant core model (front view) with detectors 2A, 3A and 2B, 3B.
12	Illustration of some quantities used.
13	The 1-4 tilt (%) transient due to a refuelling perturbation.
14	The 1-4 tilt (%) transient due to a xenon perturbation.
15	The maximum thermal flux transient due to a xenon perturbation.
16	The 1-4 tilt (%) transient due to a xenon perturbation with zone filling in steps.
17	Quadrant core model (front view) with the zone controllers and the various pairs of detectors examined.

FIGURE

18 The time response, 1-4 tilt (%), of various pairs of detectors examined, due to a xenon perturbation.

19 Relationships among the detectors.

1. INTRODUCTION

The SORGHUM[1,2] code was used to investigate the effectiveness of various arrangements of zone controller and detector locations in suppressing xenon-induced spatial power oscillation in Bruce B. Cross sections used in the CHEBY[3] code, which is a more detailed code using variable mesh spacing along each axis and thus being more expensive to run, were used as a starting point to set up an appropriate SORGHUM model. The requirement is that the steady state thermal flux distributions calculated by both codes should be as nearly the same as possible.

A quadrant core reactor model was used in the analysis (Figures 1, 2 and 3) and at first a three-dimensional search was undertaken for the optimal axial locations of the zone controllers and the various detectors. The main considerations for this were reactivity worth and effective control of various spatial modes.

A two-dimensional search was undertaken next for the optimal radial locations of the zone controllers and the detectors. A two-dimensional simulation is, of course, quite less expensive than a three-dimensional one and thus we had the capability to achieve a very detailed search for the optimal locations mentioned above.

2. DERIVATION OF THE CROSS SECTIONS

In order to use the SORGHUM code, it is necessary first to produce the proper cross sections to be used in this code. To this effect, we start with discrete incremental absorption cross sections describing the adjusters themselves as used in simulations with the CHEBY code. Then we tried to modify them appropriately so that the steady state

thermal flux distributions obtained by both codes were comparable. In this way, a good degree of confidence can be established in the results generated by the SORGHUM code.

A brief description of this code is in order here. Then the procedure of setting up its properties will be given.

SORGHUM[3] is basically a two-group neutron diffusion code. It is a code to be used for evaluation methods of controlling large power reactors during and after some prescribed perturbation. The control of the reactor can be achieved by the use of the control system, absorptive control rods or fissionable booster rods, both referred to by the single name controller. The control algorithm varies the amount of controller material in the core by increasing or decreasing the thermal absorption and fission cross sections in the controllers by amounts necessary to maintain criticality. This cross section variation can be performed either uniformly over the entire volume of a controller, or in such a way as to simulate stepwise insertion or removal of the controller. The mesh spacing must be constant in every coordinate.

Each cell of the core model contains D_2O, a fuel rod, and it can also contain an absorber rod, an adjuster, etc. Lattice parameter codes are used to generate overall cross sections for the entire cell volume, by taking into account all the physical processes involved. These cross sections are referred to as "supercell" properties.

There exist relationships between the incremental "supercell" cross sections and the discrete incremental cross sections (Figure 4). Using the curves of this Figure and the initial discrete properties (Table 1), the "supercell" properties are found (Table 2). Then, due to

the fact that the volume over which the adjuster cross sections are smeared in the SORGHUM code is different to the volume used in the computer models generating the "supercell" properties, the values found above were volume averaged as shown on Table 3.

However, when cross sections are smeared proportionally over some larger volume, we must always take into account the fact that the new "average" cross sections describe now also a part of the core with different fluxes. Thus, an adjustment is needed to conserve the reaction rates in all regions.

Assume that V_1 and V_2 are the cell volumes used in the computer codes generating the "supercell" properties and in the simulations with the SORGHUM code respectively, and assume also that Σ_1 and Σ_2 are their cross sections corresponding to the volumes above. Then one must have

$$\phi_1\Sigma_1V_1 = \phi_2\Sigma_2V_2$$

where ϕ_1 and ϕ_2 are the corresponding flux distributions. But the fluxes are higher the further away from the adjusters and thus they are higher in the larger cell (the cell of the SORGHUM model in our case). The above relationship though can be written as

$$\phi_1\Sigma_1V_1 = k\phi_2\Sigma_2V_2$$

or

$$\phi_1\Sigma_1V_1 = \phi_2(k\Sigma_2)V_2$$

i.e. an adjustment can be made in the cross sections of the SORGHUM model in order to conserve the reaction rates. That adjustment in our simulations was determined to be 0.9.

The final adjusted values used for the uniform incremental absorption cross section for adjuster rods are also listed on Table 3 along with all the material properties for the Bruce B core used in our simulations with SORGHUM.

The comparison between steady state thermal flux distributions obtained with SORGHUM and CHEBY is acceptable and is shown on Table 4.

3. THREE-DIMENSIONAL SEARCH

In this chapter a three-dimensional search for the optimal axial locations of the zone controllers and the detectors is described.

To help place the sone controllers[3,4], the fundamental, the first axial, the first azimuthal top to bottom and the first azimuthal side-to-side modes were investigated by using the SORGHUM code in x-y and x-z geometries. These modes can be seen in Figures 5 to 8. The analysis was restricted only to spatial modes corresponding to steady state reactor operation; the effect of adjuster rod movements, for example, on various model peaks was not investigated. From the modes above we concluded that the optimum axial locations of the zone contollers are $z = 8$ or $z = 9$.

To help place the in-core flux detectors[3,4], changes in thermal flux levels in the vicinity of the various zone controllers were investigated in response to individual absorber level changes in the zone controllers. Tables 5 and 6 give the ratios in zonal powers that were found corresponding to emptying the first controller. Various detector layouts were selected in which the detectors were placed at the location where the ratio of thermal flux values before and after the

control absorber level change was approximately the same as the ratio of the corresponding zonal powers. These layouts are shown in Figures 9, 10 and 11. In the same Figures, the location of the refuelling perturbation introduced subsequently is also shown.

The control action taken during and after the refuelling perturbation can fulfill either of two general requirements[3]: (1) the controllers can be set to operate similarly, so as to maintain criticality but not to control flux tilt; (2) the controllers can operate independently of one another so as to maintain criticality and prevent flux tilt due to the perturbation. This independent controller requirement is satisfied by dividing the reactor into four zones, each containing one, and only one, controller. In addition, there may be up to four detector sites in each zone.

In each one of the four control regions we obtain the time response at each detector location due to the perturbation. This search gives us a feeling of the detector locations most effectively representing the zone happenings.

The resultant transients are tabulated on Tables 7, 8, 9 and 10. From those Tables we can see that detectors 1c and 4c exhibit an acceptable performance in the control regions #1 and #4 respectively, while both sets of detectors in the middle control regions #2 and #3, i.e. detectors 2A, 3A and 2B, 2B, exhibit an also acceptable performance.

Subsequently, the effectiveness of controller configurations was evaluated. For this to be achieved we make use of two concepts by which controller-detector configuations and control schemes can be evaluated.

For a particular configuration and algorithm, we introduce an

arbitrary asymmetrical perturbation into a steady state core and thereby determine the effectiveness factor of the system. We define the effectiveness factor[3] as the ratio of the side-to-side tilt caused by the perturbation with spatial control, to the corresponding value with no spatial control. Thus, we obtain the effectiveness of the control system to compensate immediately for changes in the spatial flux distribution caused by a reactivity perturbation. This, by itself, is not sufficient and we must determine how well the spatial power distribution is maintained in time.

We continue to record the neutron flux distribution history with a specific spatial control algorithm and thus determine the figure of merit of the system. We define the Figure of Merit[3] as the ratio of the maximum side-to-side tilt caused by the perturbation. It is a measure of how uniform the spatial power distribution is maintained in time following a perturbation. The above are illustrated in Figure 12.

The side-to-side tilt is defined as follows:

$$\% \text{ side-to-side tilt} = \frac{P_L - P_R}{P_{TOTAL}} \ 100$$

where $P_{TOTAL} = P_L + P_R$ and P_L and P_R are neutron production rates in the left and right halves of the reactor respectively. P_{TOTAL} is the total neutron production rate.

The transient of the side-to-side percent flux tilt due to a refuelling perturbation is obtained when the zone controllers are at Z = 8, and with no spatial control (Table 11). On the same Table there are also the same transients with spatial control and for various

controller-detector configurations. The Effectiveness Factor (EF), Figure of Merit (FM), System Effectiveness (EF x FM), and Zone Controller worth for each case are also listed.

The two favourite controller-detector configurations, as it can be seen from Table 11, are: (1) Zone controllers at Z = 8 with detectors 1B, 4B (at Z = 10) and 2B, 3B (at Z = 12). The system effectiveness in this case is 0.033, i.e., the maximum side-to-side tilt caused by a whole channel refuelling with spatial control was reduced to 3.3% of the initial value found when no spatial control was used; (2) Zone controllers at Z = 9 and detectors 1B, 4B (at Z = 11) and 2B, 3B (at Z = 13), with a system effectiveness equal to 0.016.

Judging from the system effectiveness, the configuration (2) seems more effective than the configuration (1) in suppressing the flux tilt. However, the controller worth in that case is lower (1.758 mk compared to 2.184 mk), and thus the configuration (1) is preferred due to its higher controller worth.

4. TWO-DIMENSIONAL SEARCH

With the three-dimensional study being completed so far, we were able to draw conclusions about the optimal axial location of the zone controllers and the detectors associated with them. In order now to find the optimal radial location of the controllers and to search for the effectiveness of numerous detector locations radially, a two-dimensional analysis seems quite advantageous, due to its much lower computer cost.

Starting with the search for the best radial locations of the zone controllers, a refuelling perturbation is introduced and the transient of the percentage flux tilt between the control regions #1 and #4 is observed for three different radial locations of the zone controllers. These transients are tabulated on Table 12 and illustrated in Figure 13. It can be seen that the controllers being at x = 9 and x = 23 (Figure 13) are the most effective.

Due to the localized nature of the refuelling perturbation, a uniform xenon perturbation is in order here to establish a greater degree of confidence in our results. The corresponding transients due to such a perturbation are tabulated on Table 13 and illustrated in Figure 14. The very important conclusion from Figures 13 and 14 is that regardless whether the perturbation introduced is localized or uniform, the relative response of the three different radial locations of the zone controllers is the same. Thus, the introduction of a zenon perturbation is preferred in the rest of our analysis.

Assuming now that the zonal power information is available, or in other words, trying to maintain the power at the various zones constant, and introducing again a xenon perturbation, the transient of the thermal flux is obtained for each one of the three radial controller locations. These transients are tabulated on Table 14 and illustrated in Figure 15. Again we can see that the controllers are most effective when they are at x = 9 and x = 23.

So far we had a uniform zone filling for all the cases studied. Zone filling in steps was thus introduced and again the transient of the percentage side-to-side flux tilt was obtained due to a xenon

perturbation. These transients tabulated on Table 15 and illustrated in Figure 16 show again that the relative response of the three different radial controller locations is the same. Thus, we finally concluded that x = 9 and x = 23 were the best radial locations for the zone controllers. This being the case, a detailed search for the effectiveness of various detector locations in the vicinity of the zone controller was undertaken.

Before this was done though, it was necessary to have a good guess on the approximate area over which this search should be concentrated. To this effect and working at steady state with a power ratio equal to 1.104649, we empty the first controller and observe the power ratio at many locations around it (Table 16). The same is done for a xenon perturbation (Tables 18 and 19). Subsequently, the difference in the values of the power ratios at the various locations, as obtained by the two methods above, are computed and tabulated on Table 19. We can see that at x = 10.5 and y = 3.5 we have the least difference and we concluded that a detector should be more effective around that location. This can serve us as a starting point in our search for the most effective detector locations and the approximate region in which we should concentrate our efforts.

In Figure 17 one can see the various detector locations analyzed. The criterion used again here for the effectiveness of each location, or rather line symmetric pairs of locations since zone detectors are introduced in pairs, is the percentage side-to-side flux tilt due a xenon perturbation, identical for all cases.

The corresponding transients resulting from each pair of

detectors studied are tabulated on Table 20 and are illustrated in Figure 18.

Trying to find out whether there exists a systematic way of deciding for the most effective detector location, we plot for the various detectors, along the x-axis the maximum side-to-side percentage flux tilt due to xenon perturbation, and along the y-axis the flux ratio at the detector locations as a result of emptying the controller #1 (Figure 19).

From this Figure and from Figure 17, we observe that there is a fairly flat relationship among the detectors inward (radially) to the zone controllers, and another also flat relationship among the detectors outward to the zone controllers. Thus, we cannot select any detector locations which are significantly superior. However, one can use the relative sensitivity of the various detector locations in responding to the xenon sensitivity of the various detector locations in responding to the xenon perturbation introduced (Figure 18), in order to find the most effective detector location. From Figure 18 we can see that the detector D-2, with coordinates x = 7 and y = 3, exhibits a superior performance than the rest of the detectors. For the final decision though, the actual location availability in the reactor core must be taken into account.

REFERENCES

1. O. A. Trojan, Private Communication.

2. P. Akhtar, Y. Anastasiou, "Zone Controller and Detector Locations in Bruce B", AECL Report SLB-01, September 1975.

3. O. A. Trojan, "Space-Time Reactor Control". Paper presented at the Simulation Symposium of Reactor Dynamics and Plant Control, Toronto, May 1974.

4. P. Akhtar, "1200 MW (PHW) Zone Controller and Detector Locations-Horizontal Zone Control System", AECL Report SLB-01, September 1975.

5. V. K. Mohindra, Private Communication.

TABLES

TABLE 1

Incremental Absorption Cross-Sections

used in the Simulations with the CHEBY Code

Central Bank

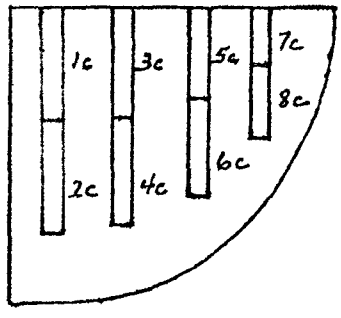

Back Bank

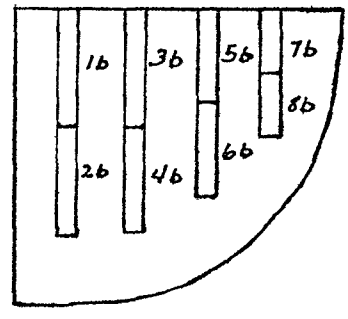

Adjuster Designation	$\Delta\Sigma a_2$ (cm^{-1})	Adjuster Designation	$\Delta\Sigma a_2$ (cm^{-1})
1c	0.0195	1b	0.0115
2c	0.0140	2b	0.0100
3c	0.0240	3b	0.0140
4c	0.0200	4b	0.0110
5c	0.0190	5b	0.0125
6c	0.0150	6b	0.0095
7c	0.0135	7b	0.0070
8c	0.0070	8b	0.0050

TABLE 2

"Supercell" Properties from Discrete Adjuster Properties

Adjuster	$\delta\Sigma a$ (discrete)	Ratio for $\delta\Sigma a_2$ (Figure 4)	Ratio for $\delta\gamma\Sigma_{f2}$ (Figure 4)	$\delta\Sigma a_2$ ("supercell")	$\delta\gamma\Sigma_{f2}$ ("supercell")
1c	1.95	0.0884	0.058	1.7238	1.1310
2c	1.40	0.090	0.067	1.2600	0.9380
3c	2.40	0.0856	0.0473	2.0544	1.13403
4c	2.00	0.0882	0.057	1.7640	1.1400
5c	1.90	0.0888	0.058	1.6872	1.1248
6c	1.50	0.0899	0.0656	1.3485	0.9840
7c	1.35	0.0899	0.0676	1.2136	0.9126
8c	0.70	0.0838	0.0834	0.5866	0.5838
1b	1.15	0.0892	0.070	1.0258	0.8050
2b	1.00	0.0884	0.0732	0.8840	0.7320
3b	1.40	0.0900	0.067	1.2600	0.9380
4b	1.10	0.0890	0.071	0.9790	0.7810
5b	1.25	0.0894	0.0688	1.1175	0.8600
6b	0.95	0.0880	0.0744	0.8360	0.7068
7b	0.70	0.0838	0.0834	0.5866	0.5838
8b	0.50	0.0762	0.0930	0.3810	0.4650

TABLE 3

Material Properties for Bruce B

(Equilibrium fuelled core; uniform time averaged lattice parameters)*

Material	Σ_{a1}, cm^{-1}	Σ_{a2}, cm^{-1} (xenon free)	$\nu\Sigma_{f2}, cm^{-1}$	Σ_{R1}, cm^{-1}
Artificial Material	10^{10}	10^{10}	0	0
Reflector	10^{-11}	8.22253×10^{-5}	0	1.00801×10^{-2}
Outer Core	7.59117×10^{-4}	3.88910×10^{-3}	4.62798×10^{-3}	7.36484×10^{-3}
Inner Core	7.58641×10^{-4}	3.91418×10^{-3}	4.60027×10^{-3}	7.36533×10^{-3}
Fresh Fuel	7.61355×10^{-4}	3.58759×10^{-3}	4.41700×10^{-3}	7.36261×10^{-3}

Incremental thermal absorption cross section for adjuster rods

(i) central bank = $2.352 \times 10^{-4} cm^{-1}$

(ii) outer banks = $1.4168 \times 10^{-4} cm^{-1}$

(In the SORGHUM code, adjuster rods in both banks are assumed to be smeared over a x-z cross section of 114.3×33.438 cm^2, while the corresponding x-z cross section used in generating the "supercell" properties is 57.15×16.719 cm^2.)

$D_1 = 1.27895$ cm $\qquad$ $D_2 = 0.949133$ cm

$\nu = 2.62$ neutrons/fission

$\lambda_1 = 2.94 \times 10^{-5} s^{-1}$

$\gamma_1 = 6.44 \times 10^{-2}$ atoms/fission

$\gamma_{xe} = 2.3 \times 10^{-3}$ atoms/fission

$\sigma_{xe} = 1.219 \times 10^{-18}$ cm^2

$\lambda_{xe} = 2.1 \times 10^{-5} s^{-1}$

* V. K. Mohindra, Private Communication, PPV Case FMPAV-01.

TABLE 4

Comparison Between Steady State Thermal Flux Distributions Obtained in SORGHUM and CHEBY*

DATA	SORGHUM	CHEBY*
Overall Form Factor	0.614	0.624
Radial Form Factor	0.875	0.865
Central Depression ($= \frac{\text{Power in the central bundle}}{\text{Maximum bundle power}}$)	0.816	0.840
Max. Bundle Power kW(th)	749.01	750
Max. Channel Power MW(th)	6.415	6.495
Reactivity worth of adjustor rods (mk)	14.472	14.97

* V. K. Mohindra, Private Communication, CHEBY Case F5CAV-19.

TABLE 5

Ratio of Thermal Flux at the Various Cells

Zone Controllers are at Z = 8. Detectors 1B, 4B, at Z = 10.

1st Contoller Empty. Power Ratio = 1.14986

	y	x = 3	x = 4
z = 5	2	1.15944	1.17531
	3	1.15470	1.16645
	4	1.14627	1.15062
z = 6	2	1.16341	1.18613
	3	1.15881	1.17714
	4	1.15024	1.16020
z = 7	2	1.16720	1.19714
	3	1.16277	1.18820
	4	1.15401	1.17041
z = 8	2	1.17027	1.20554
	3	1.16592	1.19684
	4	1.15717	1.17876
z = 9	2	1.18593	1.20527
	3	1.16782	1.19670
	4	1.15897	1.17862
z = 10	2	1.17233	1.20124
	3	1.16849	1.19270
	4	1.15967	1.18545
z = 11	2	1.17264	1.19575
	3	1.16827	1.18727
	4	1.15947	1.17023

TABLE 6

Ratio of Thermal Flux at the Various Cells

Zone Controllers are at Z = 9. Detectors 1B, 4B, at Z = 11.

1st Controller Empty. Power Ratio = 1.14833

	y	x = 3	x = 4
z = 6	2	1.15325	1.17580
	3	1.15296	1.16604
	4	1.14392	1.14911
z = 7	2	1.16396	1.18932
	3	1.15884	1.17937
	4	1.14956	1.16106
z = 8	2	1.16950	1.20316
	3	1.16455	1.19319
	4	1.15505	1.17385
z = 9	2	1.17433	1.21458
	3	1.16949	1.20484
	4	1.15985	1.18487
z = 10	2	1.17782	1.21670
	3	1.17309	1.20702
	4	1.16331	1.18694
z = 11	2	1.18008	1.21462
	3	1.17527	1.20494
	4	1.16557	1.16457
z = 12	2	1.18124	1.21074
	3	1.17647	1.20101
	4	1.16666	1.18173

TABLE 7

Change in Thermal Fluxes at Different Detector Locations due to a Refuelling Perturbation.

Control Region #1.

Time (hrs.)	% Change in Power	% Change in Flux at the Detector Locations		
		Det - 1A	Det - 1B	Det - 1C
0	6.55	9.05	8.68	6.82
1	16.58	22.22	21.14	17.56
2	33.05	43.71	41.31	34.67
3	55.02	73.15	68.18	56.24
4	75.65	101.97	93.44	74.75
5	88.79	120.65	109.55	85.95
6	94.72	128.23	116.80	92.00
7	95.97	128.26	118.18	95.00
8	94.30	123.71	115.76	95.68
9	90.56	116.20	110.59	94.23

TABLE 8

Change in Thermal Fluxes at Different Detector Locations due to a Refuelling Perturbation. Control Region #2.

Time (hrs.)	% Change in Power	% Change in Flux at the Detector Locations	
		Det - 2A	Det - 2B
0	- 1.38	- 1.28	- 1.16
1	- 2.33	- 2.15	- 2.00
2	- 4.10	- 3.88	- 3.62
3	- 7.77	- 7.60	- 7.11
4	-12.93	-12.90	-12.12
5	-16.97	-17.03	-16.13
6	-18.36	-18.47	-17.52
7	-17.43	-17.42	-16.60
8	-14.92	-14.75	-14.10
9	-11.38	-11.06	-10.60

TABLE 9

Change in Thermal Fluxes at Different Detector Locations Due to a Refuelling Perturbation. Control Region #3.

Time (hrs.)	% Change in Power	% Change in Flux at the Detector Locations	
		Det - 3A	Det - 3B
0	- 1.89	- 1.99	- 1.87
1	- 3.35	- 3.46	- 3.30
2	- 5.53	- 5.73	- 5.47
3	- 9.32	- 9.78	- 9.32
4	-14.32	-15.17	-14.47
5	-18.20	-19.32	-18.38
6	-19.66	-20.76	-19.92
7	-19.00	-19.86	-19.12
8	-16.80	-17.37	-16.76
9	-13.53	-13.78	-13.33

TABLE 10

Change in Thermal Fluxes at Different Detector Locations due to a Refuelling Perturbation. Control Region #4.

Time (hrs.)	% Change in Power	% Change in Flux at the Detector Locations		
		Det - 4A	Det - 4B	Det - 4C
0	- 5.13	- 5.53	- 5.78	- 5.93
1	-14.09	-15.89	-16.00	-15.60
2	-28.87	-32.96	-32.86	-31.60
3	-47.72	-54.26	-54.03	-51.95
4	-64.13	-72.09	-71.76	-69.26
5	-73.97	-82.32	-81.86	-79.19
6	-78.31	-87.14	-86.53	-83.71
7	-80.60	-89.26	-88.48	-85.44
8	-80.85	-89.98	-89.03	-85.65
9	-79.92	-89.79	-88.64	-84.82

TABLE 11

Transients of the side-to-side tilt in various simulations.

Corresponding Effectiveness Factors, Figures of Merit,

System Effectivenesses and Controllers Worths.

Time (hrs.)	Percent Side-to-side Tilt				
	Without spatial control	With spatial control			
	Zone Controllers (Z.C.) at Z = 8	Z.C. at Z = 8 Detectors 1C, 4C at Z = 10 and 2B, 3B at Z = 12	Z.C. at Z = 8 Detectors 1B, 4B at Z = 10 and 2B, 3B at Z = 12	Z.C. at Z = 8 Detectors 1A, 4A at Z = 10 and 2B, 3B at Z = 12	Z.C. at Z = 9 Detectors 1B, 4B at Z = 11 and 2B, 3B at Z = 13
0	-0.006	-0.006	-0.006	-0.006	-0.006
1.0	4.114	0.516	-0.070	-0.363	0.054
2.0	10.819	0.685	-0.107	-0.444	0.066
3.0	21.846	0.751	-0.130	-0.466	0.061
4.0	36.254	0.750	-0.139	-0.458	0.051
5.0	49.325	0.712	-0.137	-0.436	0.041
6.0	57.438	0.655		-0.410	
7.0	61.200	0.592			
8.0	61.807				
9.0	60.163				
Effectiveness Factor (EF)		0.1254	0.017015	0.08824	0.013126
Figure of Merit (FM)		1.4554	1.98750	1.28375	1.22222
System Effectiveness (EF)x(FM)		0.1825474	0.033787	0.11328	0.016043
Z.C. worth (mk). Empty: 3.633 mk.		-2.184	-2.184	-2.184	-1.758

TABLE 12

Percentage Flux Tilt Between Regions #1 and #4
Due to a Refuelling Perturbation, with Spatial Control,
and for Three Different Radial Controllers Locations.

Time (hrs.)	1-4 Tilt (%) Controllers at x = 9, x = 23	Controllers at x = 10, x = 22	Controllers at x = 11, x = 21
-1.0	-0.013	0.019	-0.017
0.0	0.452	0.823	1.324
1.0	0.542	1.076	1.908
2.0	0.557	1.182	2.275
3.0	0.537	1.193	2.459
4.0	0.501	1.145	2.487
5.0	0.462	1.062	2.384
6.0	0.425	0.962	2.186
7.0	0.391	0.858	1.916
8.0	0.363	0.760	1.606
9.0	0.339	0.672	1.285
10.0	0.319	0.597	0.979
11.0	0.303	0.537	0.710
12.0	0.288	0.490	0.491
13.0	0.276	0.455	0.331
14.0	0.266	0.429	0.231
15.0	0.257	0.411	0.193

TABLE 13

Percentage Flux Tilt Between the Regions #1 and #4 Due to a Xenon Perturbation, with Spatial Control, and for Different Radial Controllers Locations.

Time (hrs.)	1-4 Tilt (%) Controllers at x = 9, x = 23	Controllers at x = 10, x = 22	Controllers at x = 11, x = 21
-1.0	-0.013	0.019	0.024
0.0	0.040	0.082	0.120
1.0	0.049	0.098	0.161
2.0	0.049	0.100	0.181
3.0	0.0444	0.095	0.182
4.0	0.038	0.087	0.172
5.0	0.031	0.077	0.152
6.0	0.025	0.066	0.127
7.0	0.019	0.057	0.099
8.0	0.014	0.048	0.072
9.0	0.010	0.041	0.048
10.0	0.006	0.035	0.027

TABLE 14

Maximum Thermal Flux in Reactor After a Xenon Perturbation (.991/1.009) Trying to Maintain the Power at the Various Zones Constant

Time (hrs.)	Max. Thermal Flux (10^{14})		
	Controllers at x = 9, x = 23	Controllers at x = 10, x = 22	Controllers at x = 11, x = 21
-1.0	3.33632	3.41246	3.47672
0.0	3.33847	3.42334	3.49260
1.0	3.33733	3.42435	3.49552
2.0	3.33643	3.42374	3.49542
3.0	3.33579	3.42261	3.49400
4.0	3.33591	3.42138	3.49191
5.0	3.33593	3.42025	3.48975
6.0	3.33587	3.41925	3.48780
7.0	3.33608	3.41837	3.48597
8.0	3.33618	3.41764	3.48433
9.0	3.33625	3.41699	3.48298
10.0	3.33617	3.41645	3.48183

TABLE 15

Percentage Flux Tilt Between the Regions #1 and #4 with Zone Filling in Steps and a Xenon Perturbation of (.991/1.009).

Time (hrs.)	1-4 Tilt (%) Controllers at x = 9, x = 23	Controllers at x = 10, x = 22	Controllers at x = 11, x = 21
-1.0	0.004	0.012	0.025
0.0	0.218	0.267	0.444
1.0	0.245	0.323	0.612
2.0	0.241	0.332	0.694
3.0	0.225	0.316	0.708
4.0	0.207	0.289	0.673
5.0	0.190	0.258	0.605
6.0	0.175	0.228	0.517
7.0	0.163	0.200	0.423
8.0	0.153	0.177	0.330
9.0	0.144	0.157	0.226
10.0	0.127	0.141	0.102

TABLE 16

A Section of the X-Y Plane of the Core around Controller #1.

Comparison between the Steady State Case and the Case with the

1st Controller Empty. The Power Ratio is 1.104649.

y \ x	5	6	7	8	9	10	11	12
1	1.13474	1.13860	1.14484	1.15552		1.14716	1.11861	1.09204
2	1.13279	1.13617	1.14173	1.15155		1.14246	1.11374	1.08746
3	1.12825	1.13037	1.13447	1.14241		1.13196	1.10334	1.07806
4	1.11967	1.11961	1.12091	1.12554		1.11372	1.08673	1.06419
5	1.10703	1.10274	1.09691	1.08942		1.07783	1.06269	1.04668
6								

TABLE 17

A Section of the X-Y Plane of the Core Around Controller #1

with the Effect of a Xenon Perturbation (.991/1.009) on the Fluxes.

The Power Ratio is 1.02604.

y \ x	5	6	7	8	9	10	11	12
1	1.02428	1.03314	1.03212	1.03212		1.02864	1.02604	1.02282
2	1.03313	1.03247	1.03144	1.02999		1.02802	1.02548	1.02238
3	1.03188	1.03130	1.03019	1.02874		1.02681	1.02445	1.02150
4	1.03021	1.02951	1.02850	1.02708		1.02529	1.02309	1.02035
5	1.02811	1.02739	1.02657	1.02525		1.02364	1.02157	1.01899
6								

TABLE 18

The Same as Table 17, after Normalization

to the Power Ratio 1.104649.

y \ x	5	6	7	8	9	10	11	12
1	1.10275	1.11229	1.11120	1.10958	1.10745	1.10465	1.10118	
2	1.11228	1.11157	1.11046	1.10890	1.10678	1.10405	1.10071	
3	1.11094	1.11031	1.10912	1.10756	1.10548	1.10294	1.09976	
4	1.10914	1.10838	1.10730	1.10577	1.10384	1.10147	1.09852	
5	1.10688	1.10610	1.10522	1.10380	1.10206	1.09984	1.09706	
6								

TABLE 20

Percentage Flux Tilt between the Regions #1 and #4 as seen by Various Pairs of Detectors. Controllers are at z = 8 and the Xenon Perturbation is (.991/1.009).

Time (hrs.)	1-4 Tilt (%)											
	Det-1	Det-2	Det-3	Det-4	Det-5	Det-6	Det-7	Det-8	Det-9	Det-10	Det-11	Det-12
-1.0	-0.013	-0.013	-0.013	-0.013	-0.013	-0.013	-0.013	-0.013	-0.013	-0.013	-0.013	-0.013
0.0	0.039	0.063	0.032	0.032	0.009	0.030	0.029	0.033	0.038	0.020	0.000	0.047
1.0	0.040	0.075	0.045	0.048	0.012	0.042	0.048	0.043	0.053	0.026	0.012	0.052
2.0	0.035	0.073	0.048	0.052	0.011	0.042	0.052	0.043	0.055	0.024	0.015	0.049
3.0	0.028	0.066	0.045	0.050	0.008	0.039	0.051	0.039	0.052	0.020	0.014	0.042
4.0	0.022	0.057	0.038	0.043	0.005	0.033	0.044	0.033	0.045	0.016	0.010	0.035
5.0	0.018	0.047	0.031	0.035	0.002	0.026	0.034	0.027	0.036	0.012	0.006	0.029
6.0	0.015	0.039	0.024	0.026	0.000	0.020	0.025	0.020	0.028	0.008	0.002	0.024
7.0	0.012	0.031	0.017	0.019	0.001	0.014	0.018	0.015	0.020	0.005	0.002	0.019
8.0	0.010	0.024	0.011	0.012	0.003	0.009	0.011	0.010	0.014	0.003	0.005	0.015
9.0	0.008	0.018	0.006	0.006	0.004	0.005	0.005	0.006	0.008	0.000	0.008	0.011
10.0	0.006	0.013	0.002	0.001	0.005	0.001	0.001	0.002	0.003	0.002	0.010	0.008

TABLE 21

The Flux Ratio after emptying the controller #1 and the maximum 1-4 tilt (%) for each detector location examined.

Detector #	Flux Ratio Emptying the Controller 1	Maximum 1-4 Tilt (%)
1	1.10334	0.040
2	1.13447	0.075
3	1.13569	0.048
4	1.13895	0.052
5	1.09565	0.012
6	1.10060	0.042
7	1.14034	0.052
8	1.13242	0.043
9	1.10296	0.055
10	1.12634	0.026
11	1.13037	0.015
12	0.12769	0.052

FIGURES

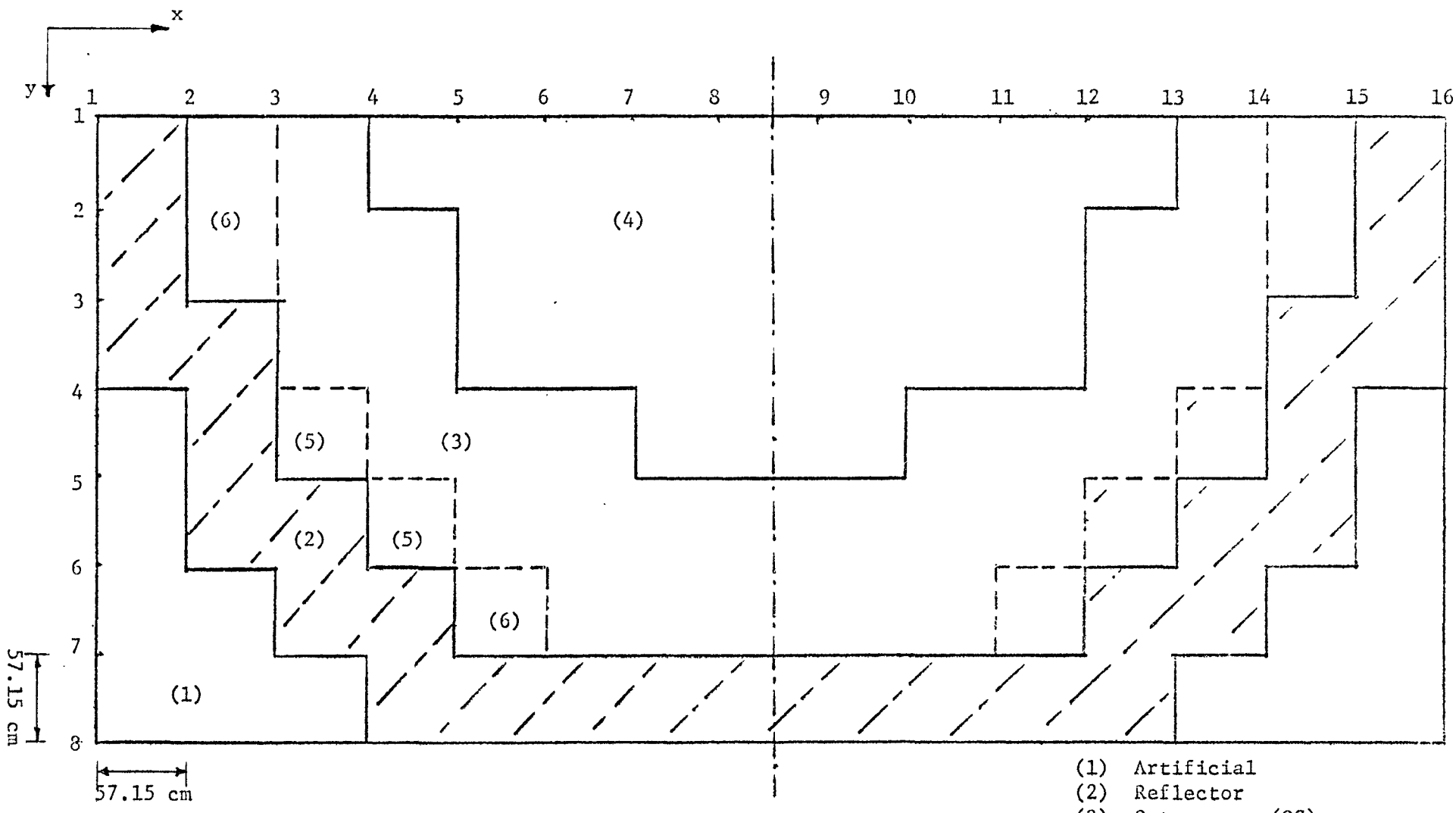

Figure 1. Quadrant core model with no adjusters (front view).

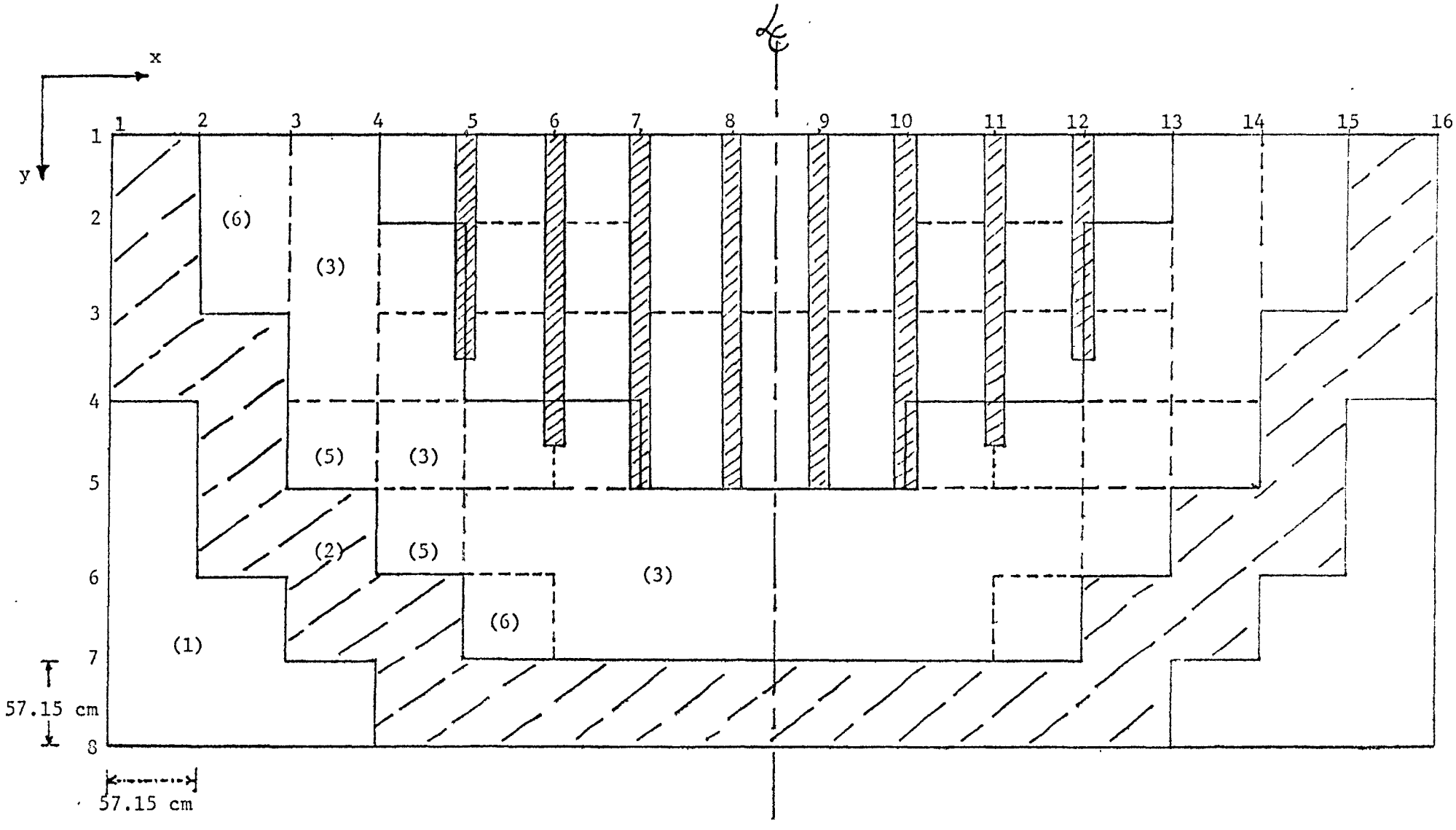

Figure 2. Quadrant core model with adjusters.

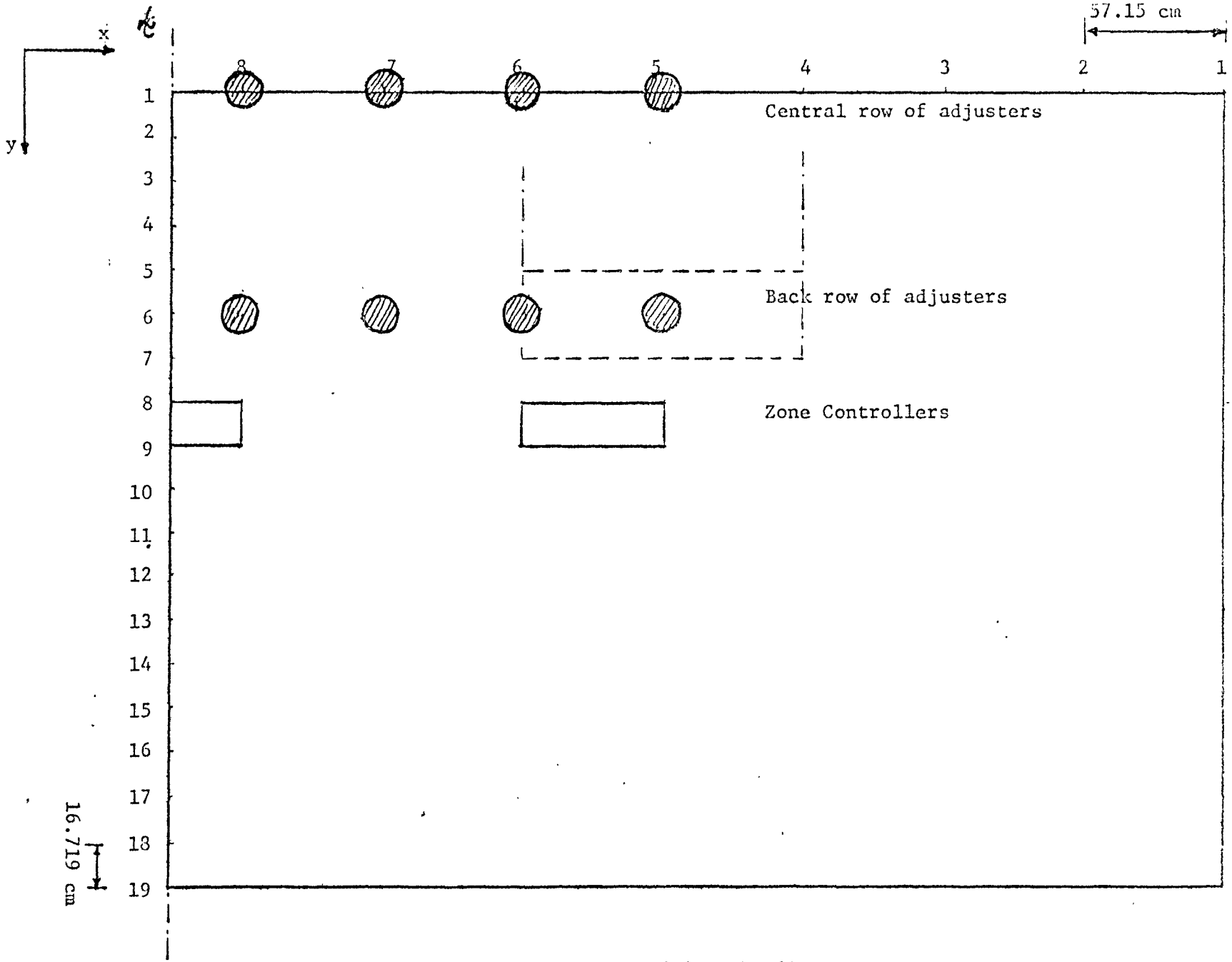

Figure 3. Octant core model with adjusters.

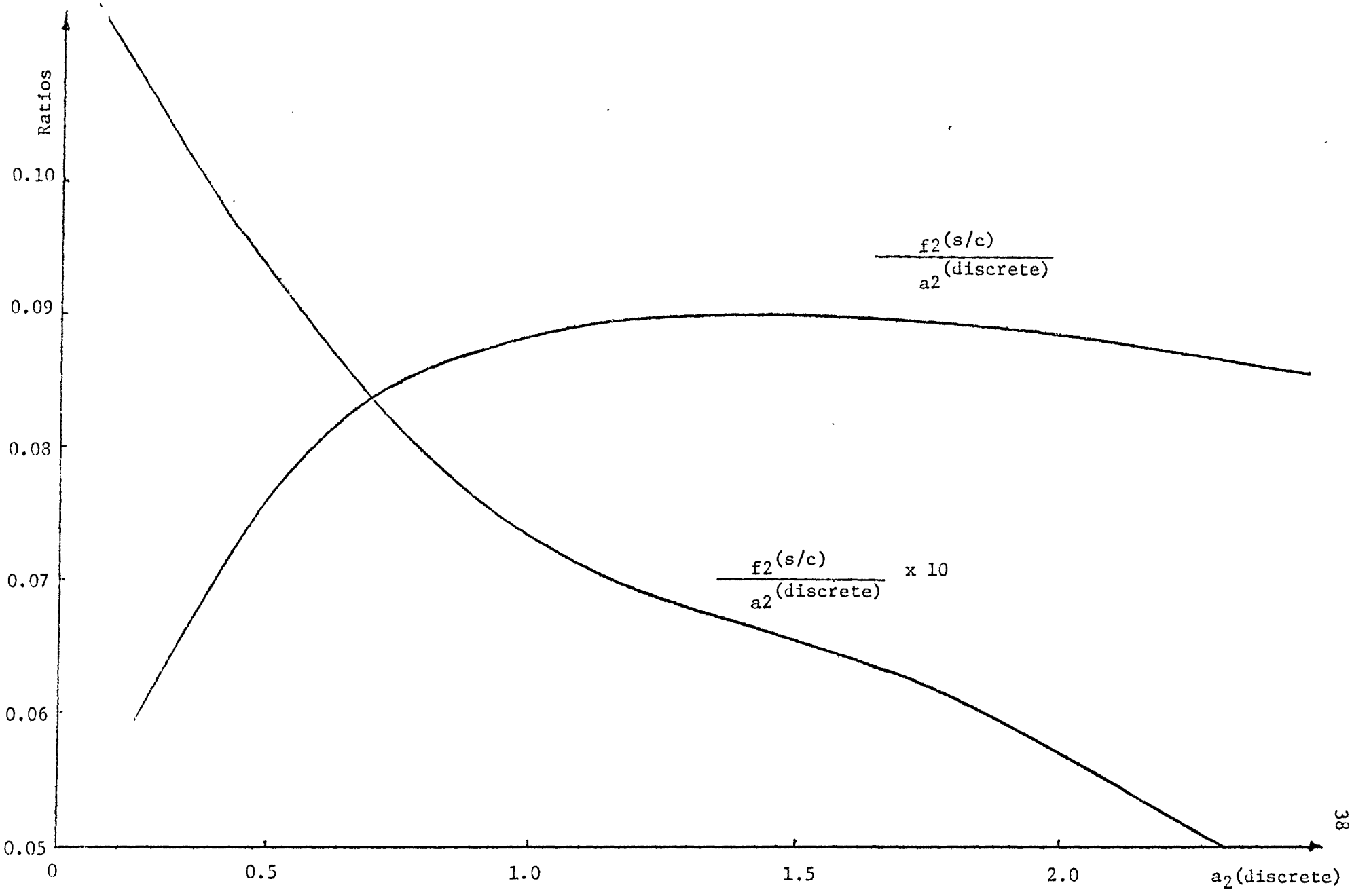

Figure 4. "Supercell" properties from discrete adjuster properties.
(C. Bailey, AECL, private communication)

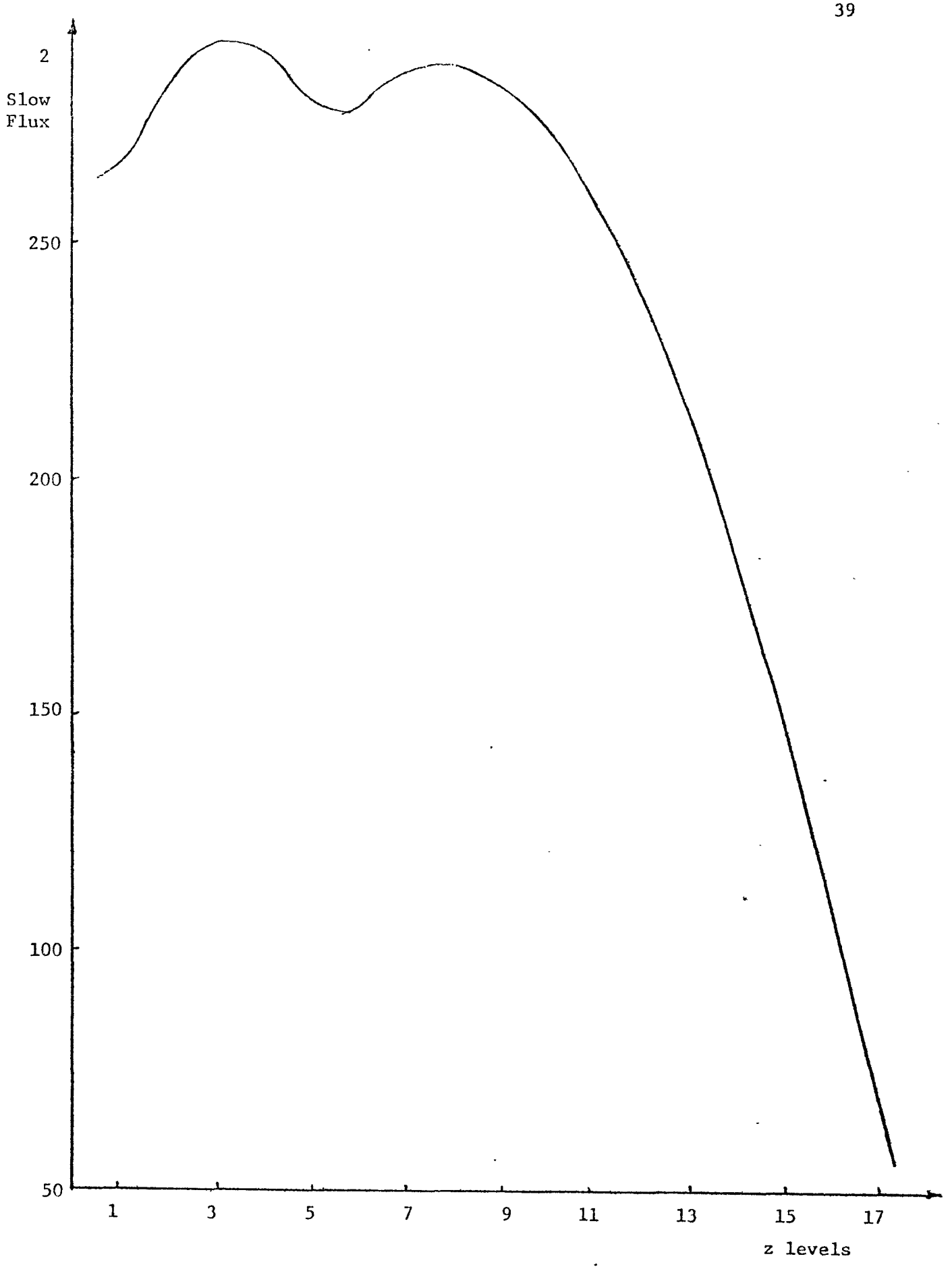

Figure 5. The fundamental mode at steady state.

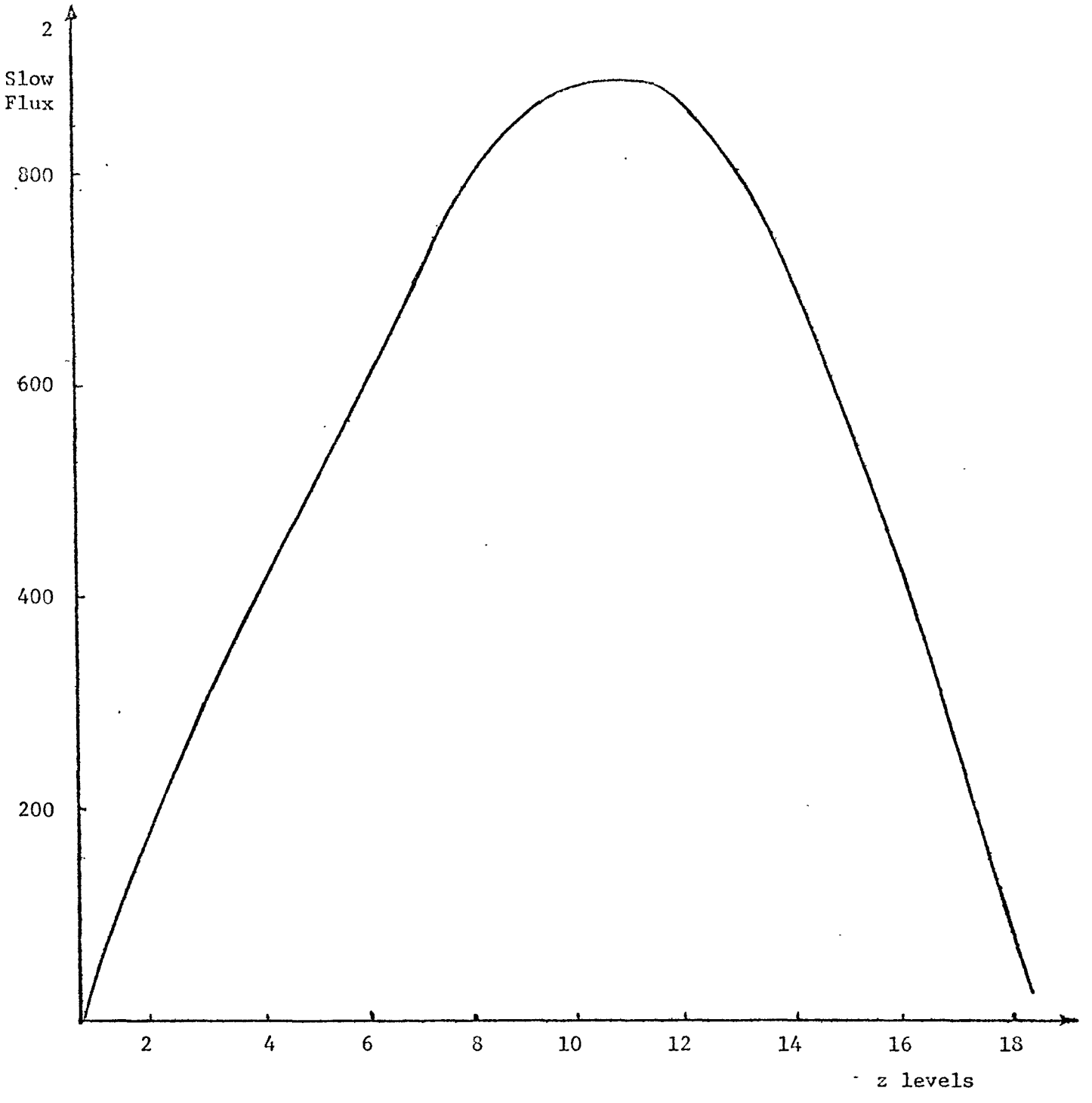

Figure 6. The first axial mode.

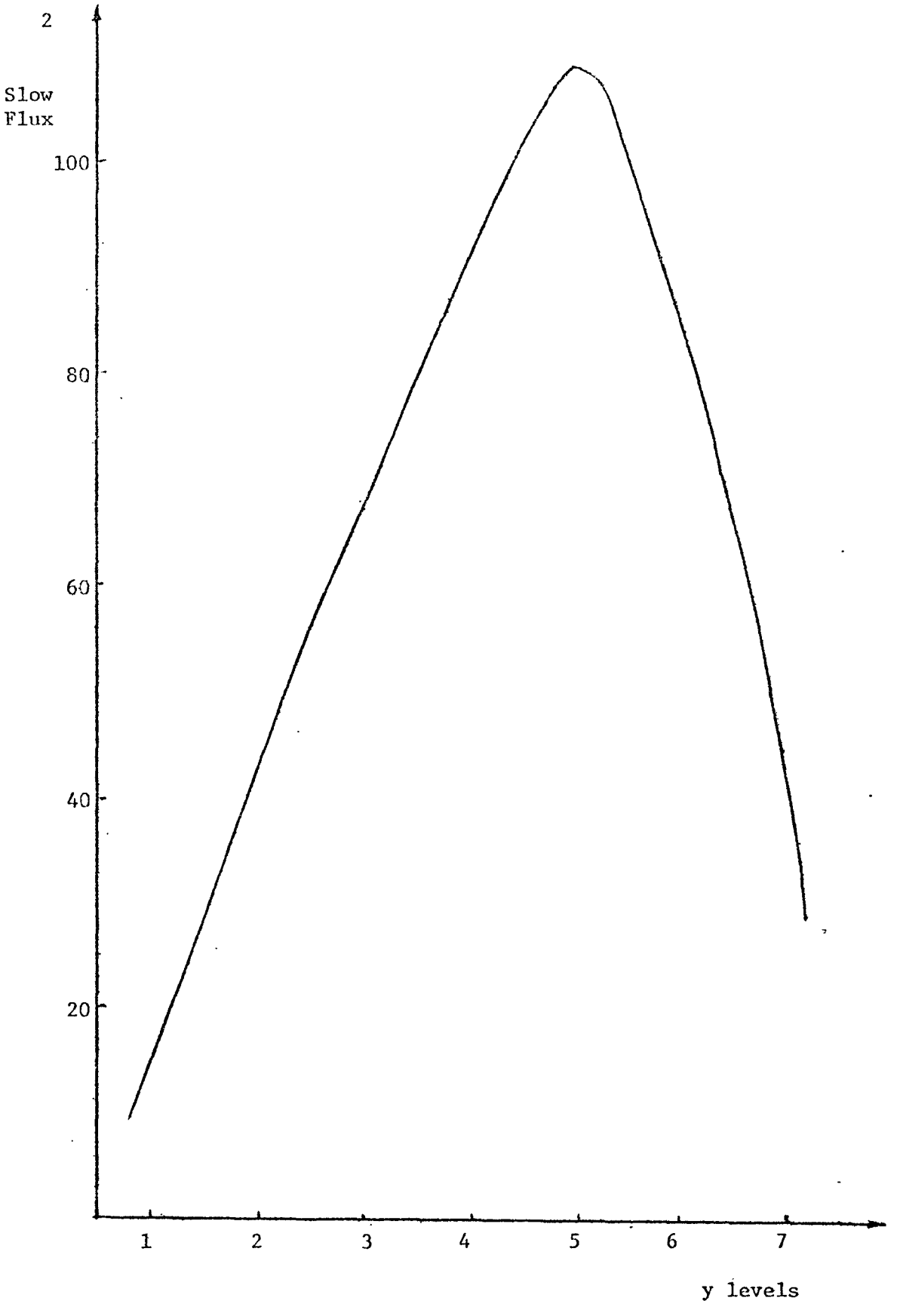

Figure 7. The first azimuthal mode (top to bottom)

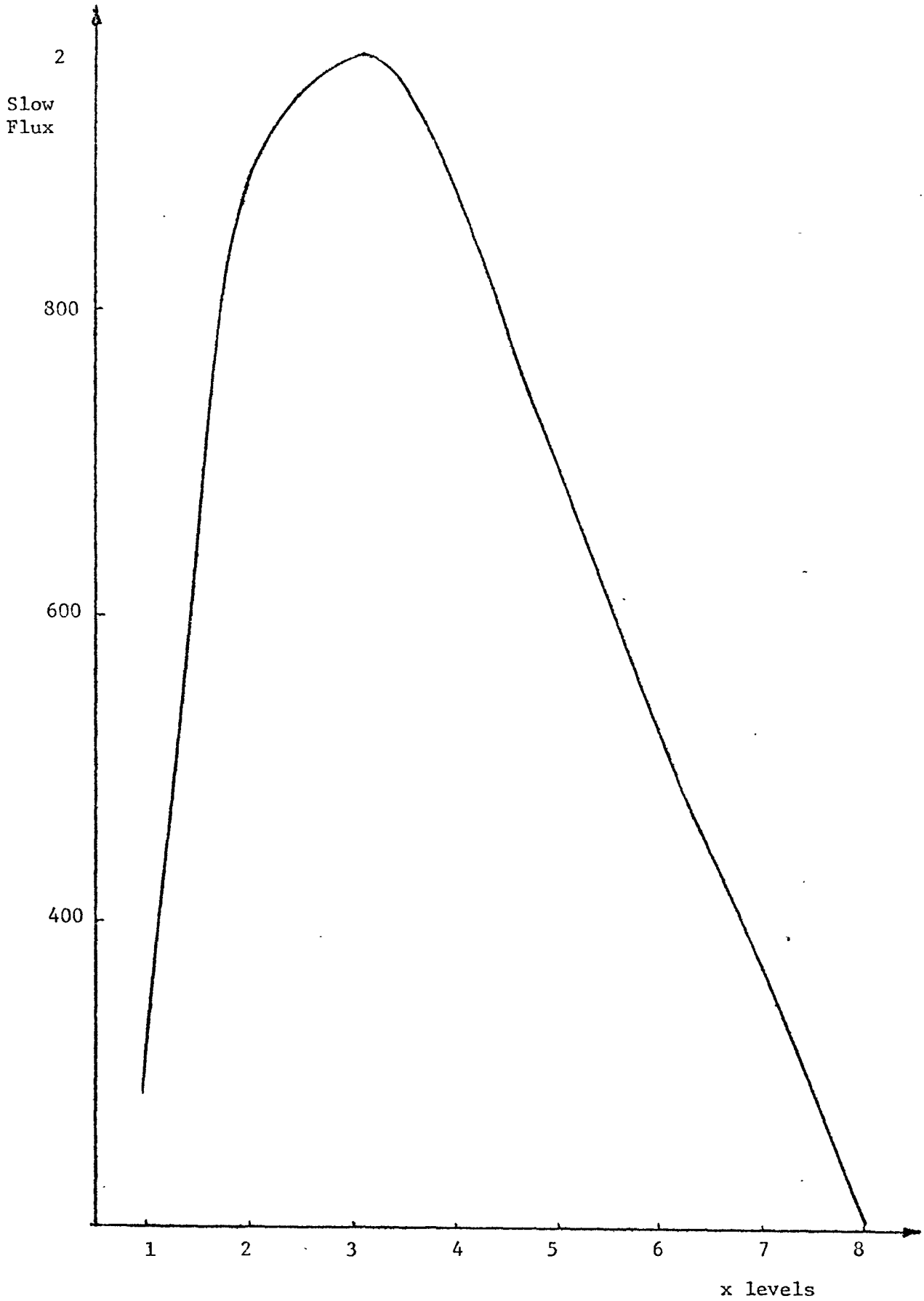

Figure 8. The first azimuthal mode (side-to-side)

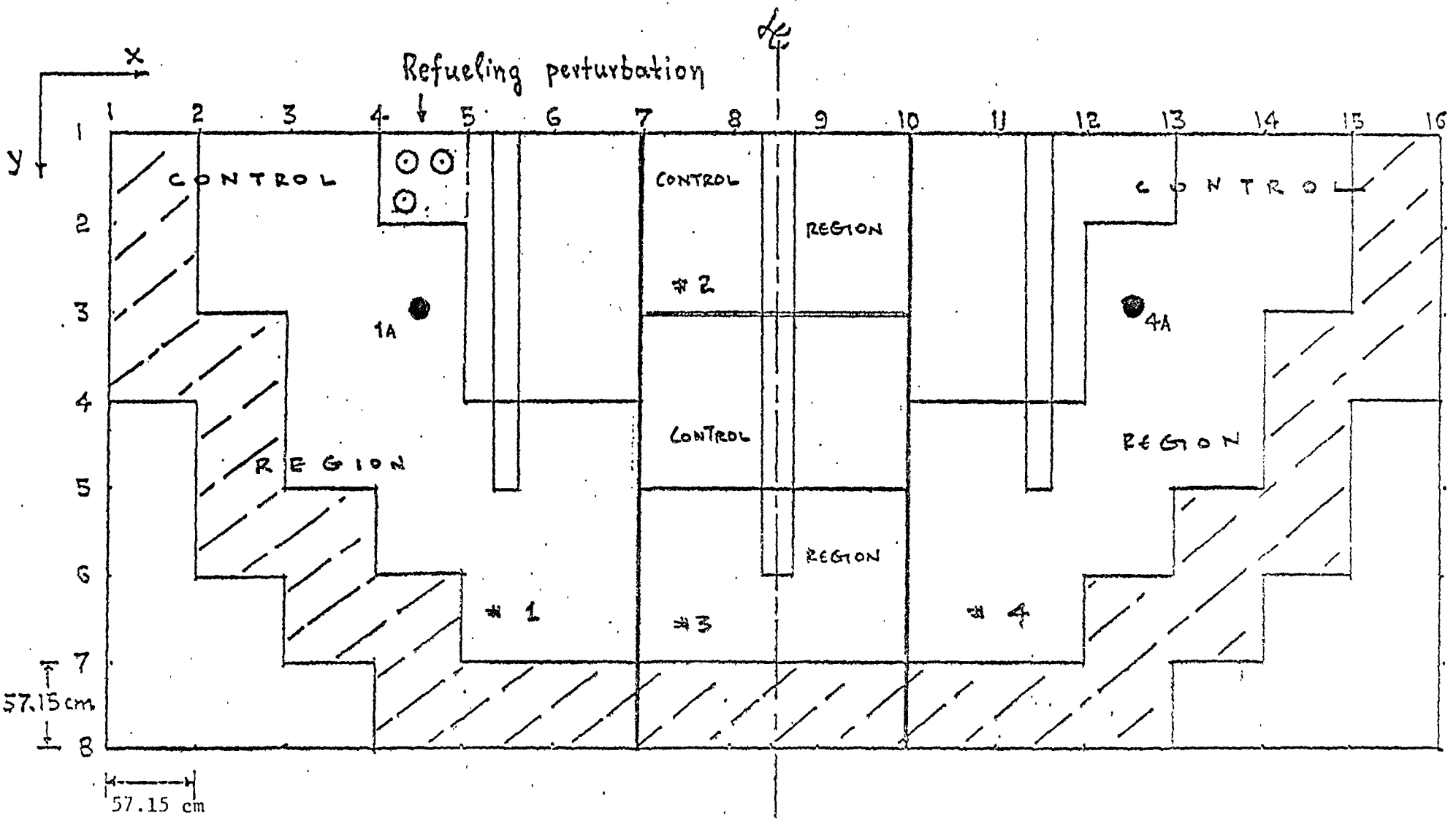

Figure 9. Quadrant core model (front view) with zone controllers and detectors 1A, 4A.

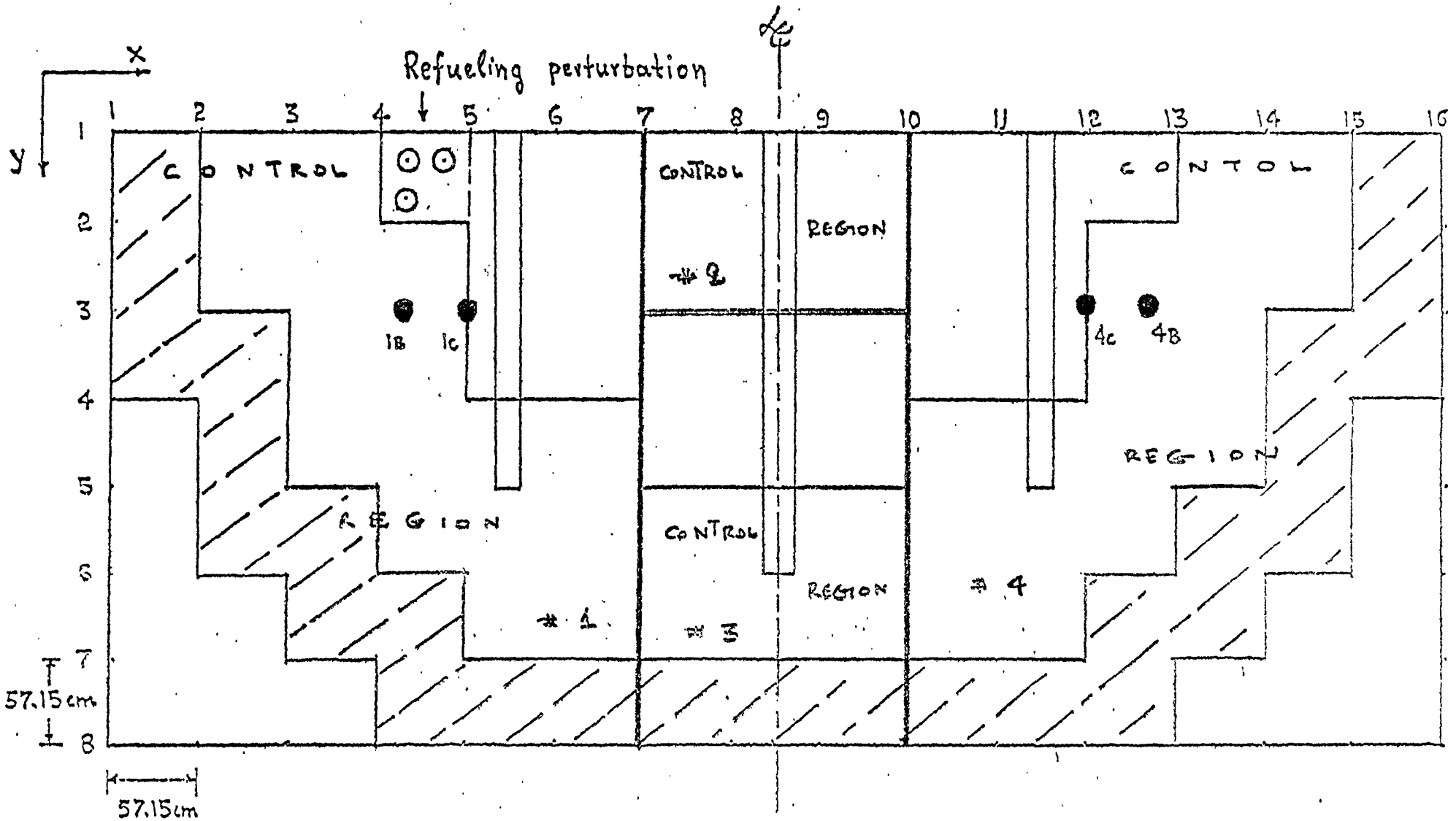

Figure 10. Quadrant core model (front view) with zone controllers and detectors 1B, 1C, 4B and 4C.

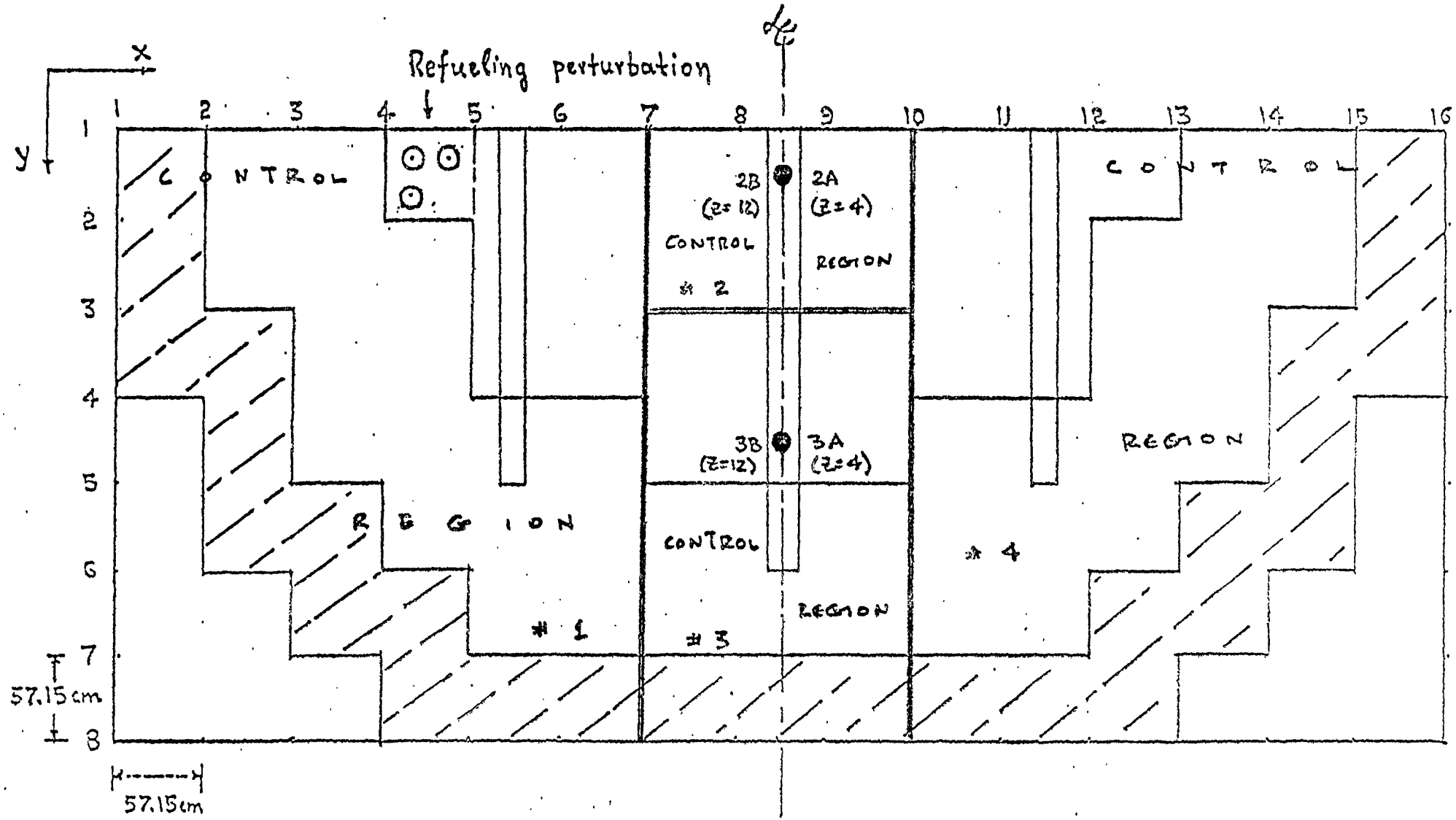

Figure 11. Quadrant core model (front view) with zone controllers and detectors 2A, 3A and 2B, 3B.

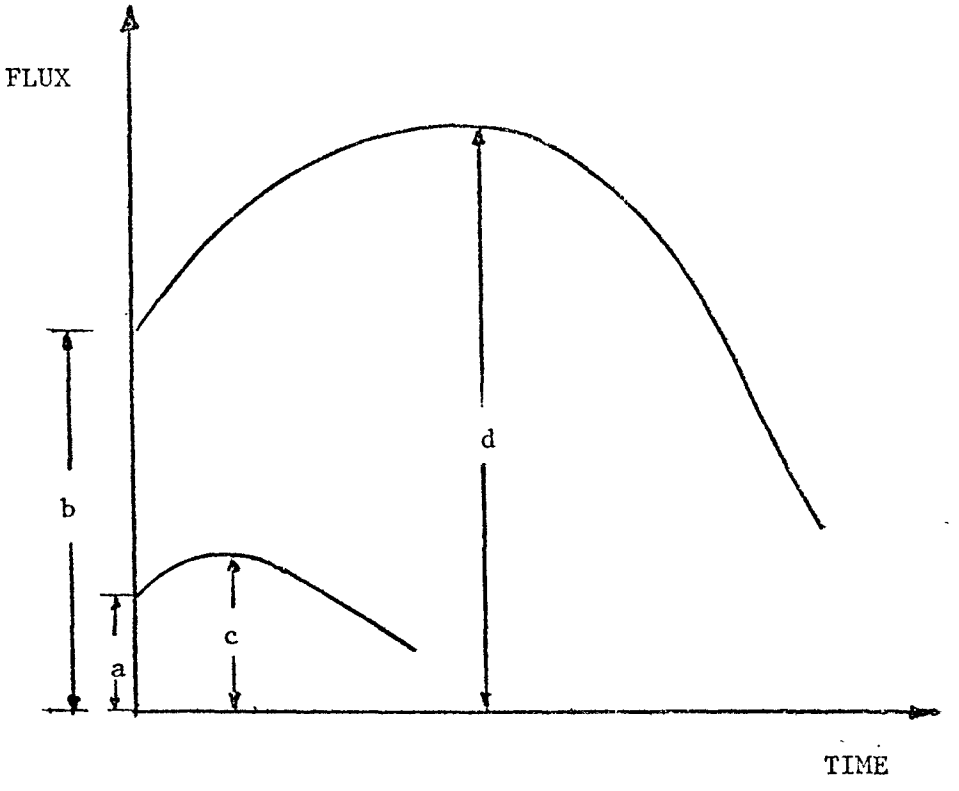

Figure of Merit (FM) = $\frac{c}{a}$

Effectiveness Factor (EF) = $\frac{a}{b}$

System Effectiveness (FM x EF) = $\frac{c}{b}$

Figure 12. Illustration of some quantities used.

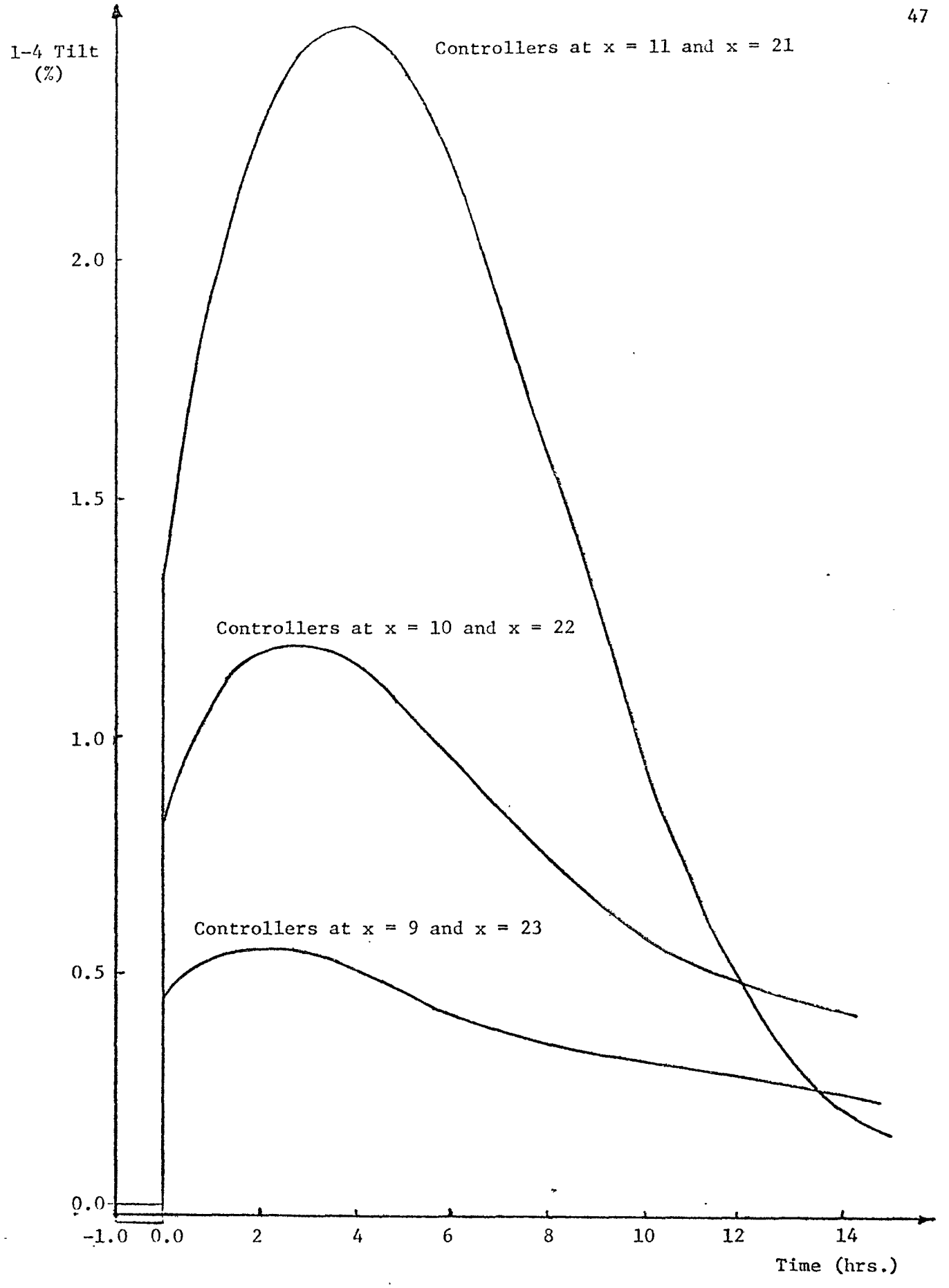

Figure 13. 1-4 Tilt (%) due to a refuelling perturbation, with spatial control and for three different radial controller locations.

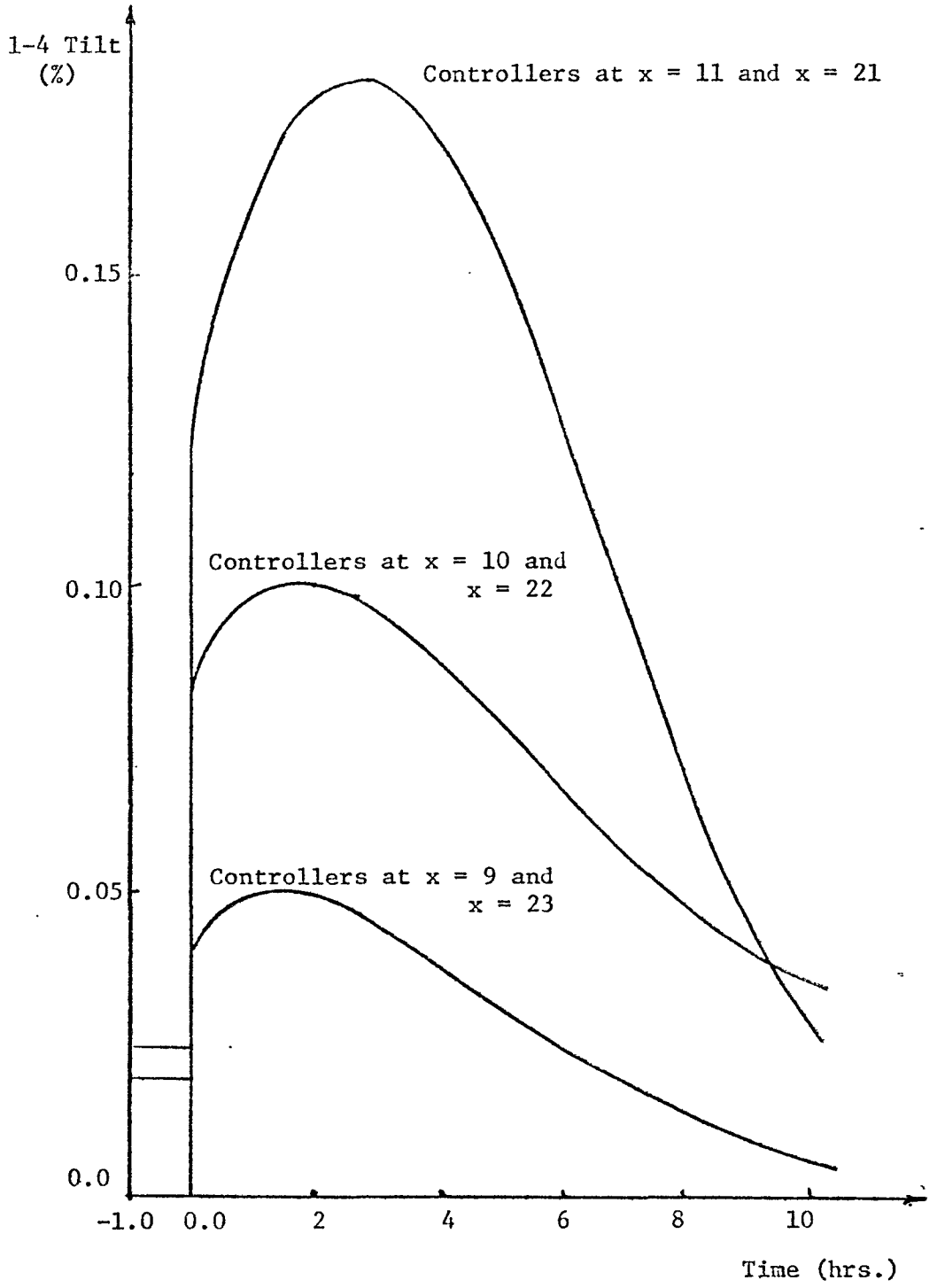

Figure 14. 1-4 Tilt (%) due to a xenon perturbation, with spatial control and for three different radial controller locations.

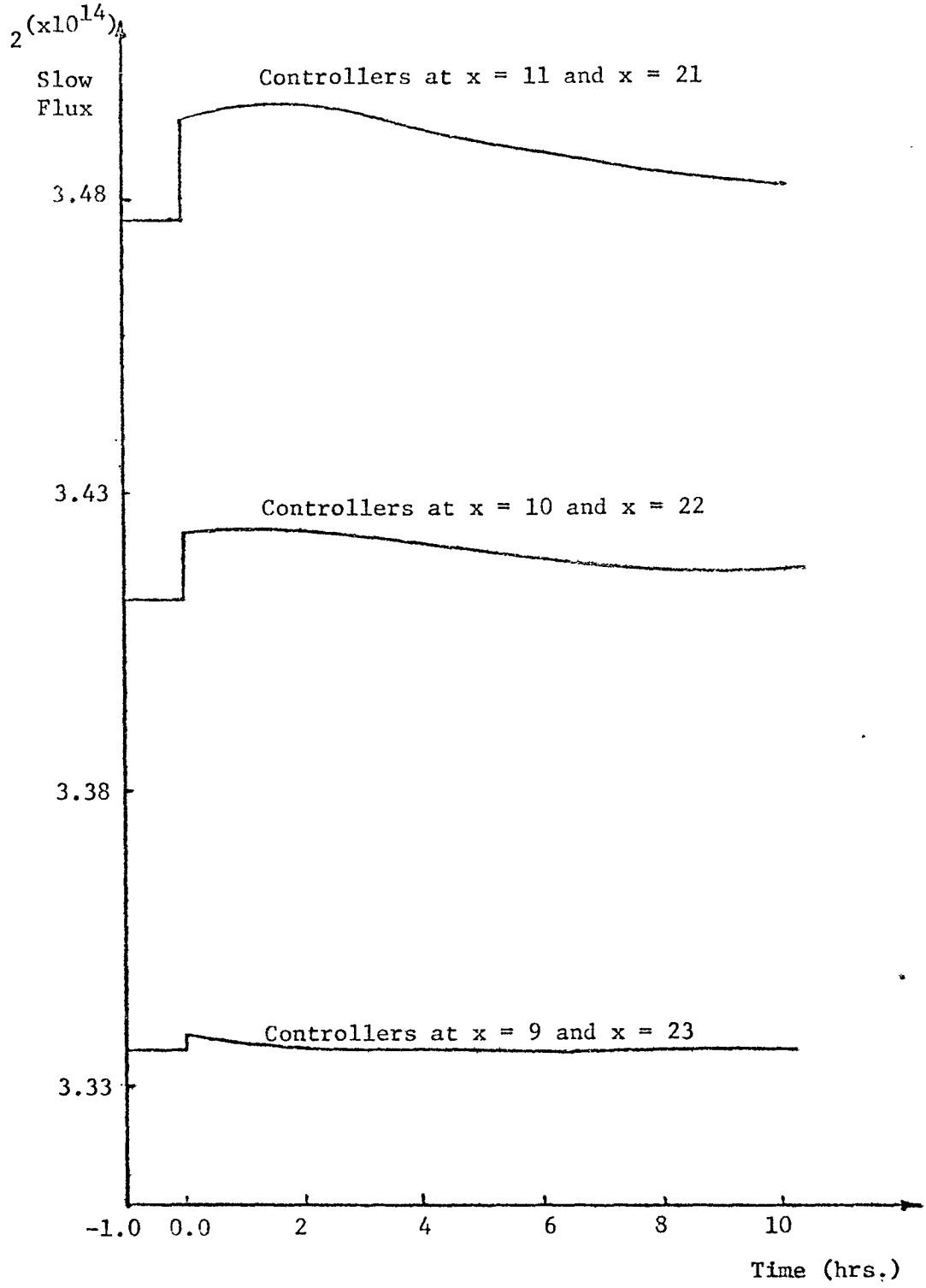

Figure 15. Maximum thermal flux after a xenon perturbation, trying to maintain constant power at the various zones.

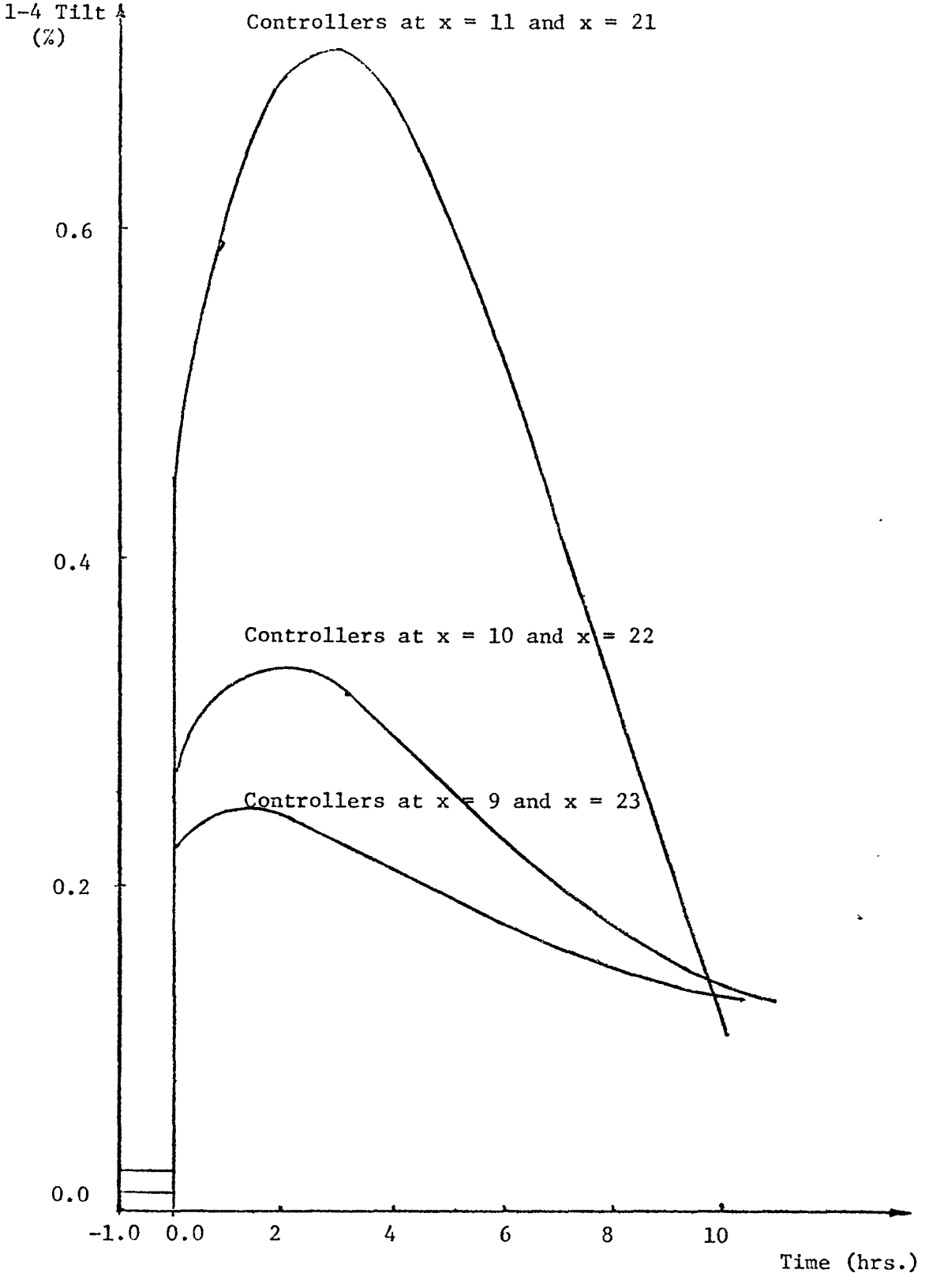

Figure 16. 1-4 Tilt (%) due to a xenon perturbation with zone filling in steps and for three different radial controller locations.

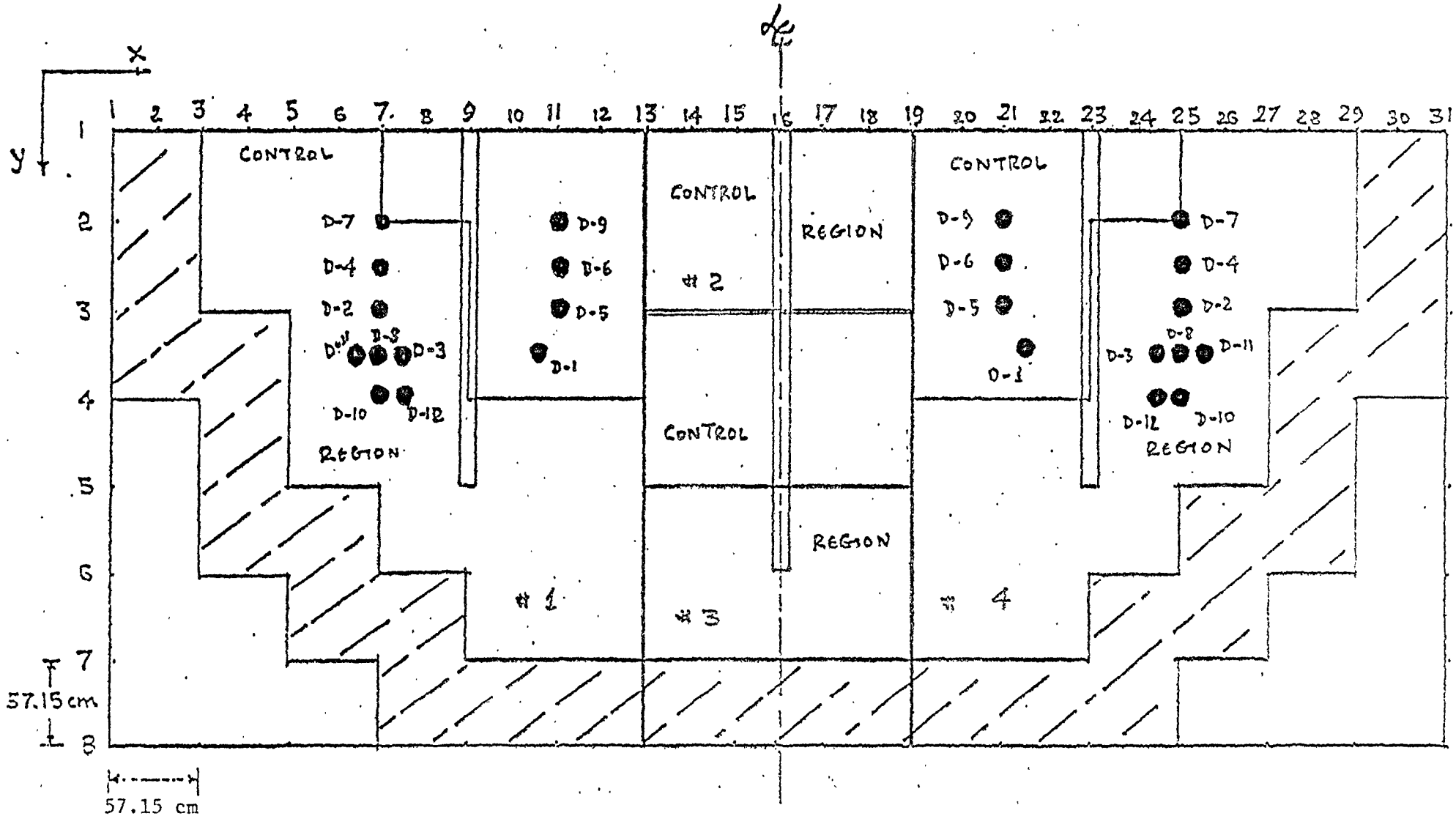

Figure 17. Quadrant core model (front view) with the zone controllers at their optimal location and the various pairs of detectors examined.

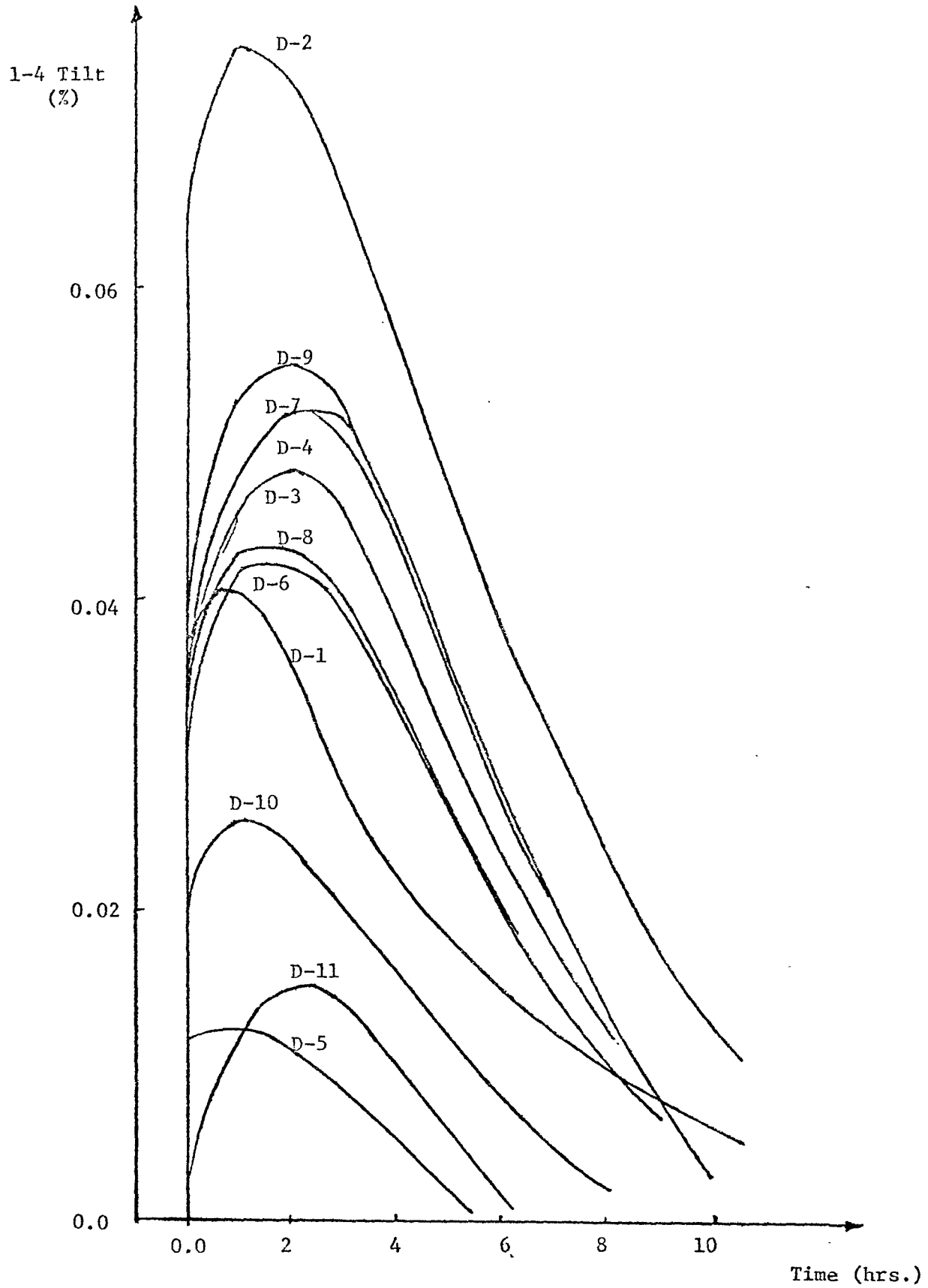

Figure 18. The time response, 1-4 tilt (%), of various pairs of detectors due to a xenon perturbation of (.991/1.009). The zone controllers are at z = 8, x = 9 and x = 23.

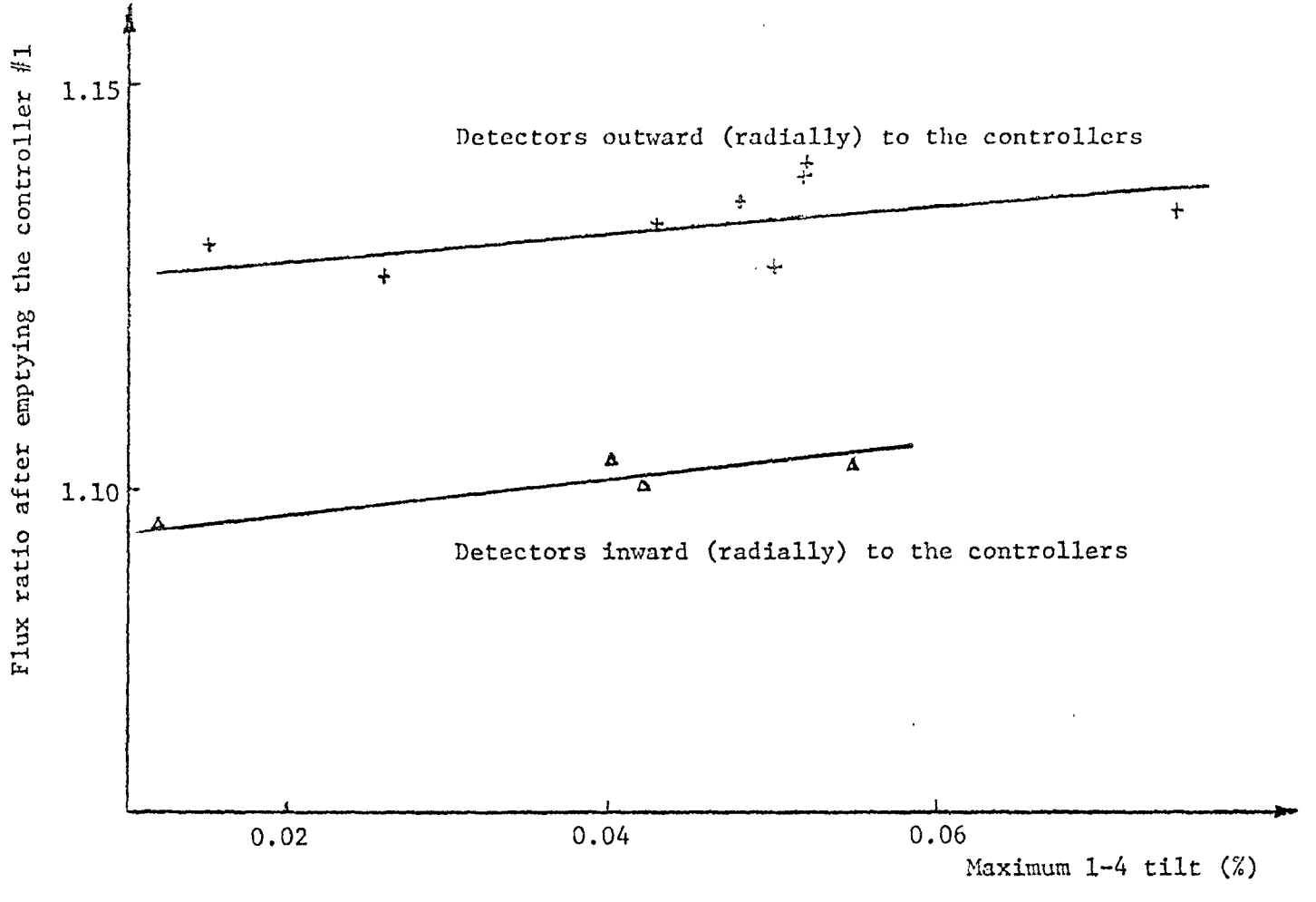

Figure 19. Relationships among the detectors.